Embedding of cortical representations by the superficial patch system

Muir, D R ; Da Costa, N M A ; Girardin, C C ; Naaman, S ; Omer, D B ; Ruesch, E ; Grinvald, A ; Douglas, R J

Abstract: Pyramidal cells in layers 2 and 3 of the neocortex of many species collectively form a clustered system of lateral axonal projections (the superficial patch system-Lund JS, Angelucci A, Bressloff PC. 2003. Anatomical substrates for functional columns in macaque monkey primary visual cortex. Cereb Cortex. 13:15-24. or daisy architecture-Douglas RJ, Martin KAC. 2004. Neuronal circuits of the neocortex. Annu Rev Neurosci. 27:419-451.), but the function performed by this general feature of the cortical architecture remains obscure. By comparing the spatial configuration of labeled patches with the configuration of responses to drifting grating stimuli, we found the spatial organizations both of the patch system and of the cortical response to be highly conserved between cat and monkey primary visual cortex. More importantly, the configuration of the superficial patch system is directly reflected in the arrangement of function across monkey primary visual cortex. Our results indicate a close relationship between the structure of the superficial patch system and cortical responses encoding a single value across the surface of visual cortex (self-consistent states). This relationship is consistent with the spontaneous emergence of orientation response-like activity patterns during ongoing cortical activity (Kenet T, Bibitchkov D, Tsodyks M, Grinvald A, Arieli A. 2003. Spontaneously emerging cortical representations of visual attributes. Nature. 425:954-956.). We conclude that the superficial patch system is the physical encoding of self-consistent cortical states, and that a set of concurrently labeled patches participate in a network of mutually consistent representations of cortical input.

DOI: https://doi.org/10.1093/cercor/bhq290

Cerebral Cortex October 2011;21:2244–2260
doi:10.1093/cercor/bhq290
Advance Access publication March 7, 2011

Embedding of Cortical Representations by the Superficial Patch System

Dylan Richard Muir[1,2], Nuno M. A. Da Costa[1], Cyrille C. Girardin[3], Shmuel Naaman[4], David B. Omer[4], Elisha Ruesch[1], Amiram Grinvald[4] and Rodney J. Douglas[1]

[1]Institute of Neuroinformatics, University of Zürich and ETH Zürich, CH-8057 Zürich, Switzerland, [2]Brain Research Institute, University of Zürich, CH-8057 Zürich, Switzerland, [3]Neurobiology, University of Konstanz, 78457 Konstanz, Germany and [4]Department of Neurobiology, Weizmann Institute of Science, 76100 Rehovot, Israel

Address correspondence to Dylan Muir, Brain Research Institute, University of Zürich, Irchel, Winterthurerstrasse 190, CH-8057 Zürich, Switzerland. Email: muir@hifo.uzh.ch.

Pyramidal cells in layers 2 and 3 of the neocortex of many species collectively form a clustered system of lateral axonal projections (the superficial patch system—Lund JS, Angelucci A, Bressloff PC. 2003. Anatomical substrates for functional columns in macaque monkey primary visual cortex. Cereb Cortex. 13:15–24. or daisy architecture—Douglas RJ, Martin KAC. 2004. Neuronal circuits of the neocortex. Annu Rev Neurosci. 27:419–451.), but the function performed by this general feature of the cortical architecture remains obscure. By comparing the spatial configuration of labeled patches with the configuration of responses to drifting grating stimuli, we found the spatial organizations both of the patch system and of the cortical response to be highly conserved between cat and monkey primary visual cortex. More importantly, the configuration of the superficial patch system is directly reflected in the arrangement of function across monkey primary visual cortex. Our results indicate a close relationship between the structure of the superficial patch system and cortical responses encoding a single value across the surface of visual cortex (self-consistent states). This relationship is consistent with the spontaneous emergence of orientation response–like activity patterns during ongoing cortical activity (Kenet T, Bibitchkov D, Tsodyks M, Grinvald A, Arieli A. 2003. Spontaneously emerging cortical representations of visual attributes. Nature. 425:954–956.). We conclude that the superficial patch system is the physical encoding of self-consistent cortical states, and that a set of concurrently labeled patches participate in a network of mutually consistent representations of cortical input.

Keywords: cat, intrinsic optical imaging, macaque monkey, primary visual cortex, spatial statistics

Introduction

The clustered arrangement formed collectively by axonal projections of pyramidal cells in the superficial layers of mammalian cortex has drawn the attention of neuroanatomists and modelers for many years. Focal injections of neural tracers reveal the tendency for populations of labeled cells to collectively form patches of labeled somata and excitatory axonal terminals, separated by regions of light or absent label, and covering several millimeters within a cortical area (Rockland and Lund 1981, 1983; Rockland et al. 1982; Lund et al. 2003). The individual pyramidal cell axonal arbors that form the assumed substrate for these patches can span at least 4 mm in cat area 17 (Gilbert and Wiesel 1983) and at least 2 mm in macaque monkey area V1 (McGuire et al. 1991). Known as the superficial patch system, the quasiperiodic nature of the labeling patterns in primary visual cortex is evocative of the petals of a flower, inspiring the alternate moniker of the daisy architecture (Douglas and Martin 2004).

Several aspects of this anatomical system are interesting, not the least of which is its apparent ubiquity across many cortical areas, in many species (see Table 1). The periodic representation used by primary visual cortex to process spatially distributed input makes the existence of periodic anatomical modules there unsurprising. However, there is no obvious reason why prefrontal cortex, which deals with information that is presumably nonspatial in nature, should require a repeated, punctate arrangement of either function or anatomy. The characteristic size and spacing of labeled patches in a given area, irrespective of the size of the injection made, has also baffled researchers (Muir and Douglas 2010; for a review, see Lund et al. 2003).

It is unclear what general principle of cortical processing is subserved by the patterned excitatory projections of the patch system. Where comparisons between patches and cortical function have been made, a consistent—albeit weak—correlation between the locations of labeled patches and markers for cortical function has emerged. In primary visual cortex, 60–75% of labeled patches fall in regions responsive to stimulus orientations within ±45° of the preferred orientation of neurons at the injection site in tree shrew (Bosking et al. 1997), cat (Schmidt et al. 1997), and macaque monkey (Malach et al. 1993; Stettler et al. 2002). The functional specificity of these connections is therefore considerably broader than the physiological orientation tuning of the projecting neurons. Nevertheless, the existence of a similar tendency for other aspects of function in visual cortex, and in other cortical areas entirely, has lead to the simplified concept of "like-connects-to-like" (Mitchison and Crick 1982).

If connectivity between related functional domains is truly the principle underlying the anatomy of the patch system, then the average spatial arrangement of the patch system and of functional maps should be identical. Previous analyses of these spatial arrangements have been restricted to comparisons made in single animals, and their accuracy has been limited by the precision of alignment between functional maps and tissue processed for histology. Here, we introduce a technique that does not rely on such alignment but directly measures the statistical structure inherent in the arrangement of labeled patches and of cortical responses. The lattice structure measured by our method allows us to compare the spatial configuration of anatomical and functional modules between animals and indeed between species. By pooling measurements of the lattice structure of the patch system across animals, we gain more sensitivity when comparing the patch system with the lattice structure of maps of the cortical response.

If the spatial arrangement of functional domains and of patches is similar, that would strongly imply a role for the

Table 1
List of observations of patchy labeling in cortex

Animal	Cortical area	Width (mm)	Spacing (mm)	References
Cat	Area 17	0.3–0.55	0.6–1.25	Gilbert and Wiesel (1983), Luhmann et al. (1986), Gilbert and Wiesel (1989), Callaway and Katz (1990), Luhmann et al. (1990), Kisvárday and Eysel (1992), Löwel and Singer (1992), Lübke and Albus (1992a, 1992b), and Kisvárday et al. (1997)
	Area 18	0.35–0.65	1–1.5	Matsubara et al. (1985, 1987), Boyd and Matsubara (1991), and Kisvárday et al. (1997)
	Area A1			Matsubara and Phillips (1988), Wallace et al. (1991), Read et al. (2001), and Ojima and Takayanagi (2004)
Ferret	Area 17	0.25	0.6–0.7	Rockland (1985b) and Ruthazer and Stryker (1996)
	Area A1	0.25–0.8		Wallace and Bajwa (1991)
Gray squirrel	Areas 17 and 18			Kaas et al. (1989) but for a conflicting report, see Van Hooser et al. (2006)
Macaque monkey	Area 1	0.375	0.8	Juliano et al. (1989) and Lund et al. (1993)
	Area 3b	0.33	0.795	Juliano et al. (1989) and Lund et al. (1993)
	Area 4	0.5–0.57	0.9–0.95	Lund et al. (1993)
	Area 7a	0.31	0.967	Amir et al. (1993)
	Areas 9 and 46	0.27–0.4	0.54–0.78	Lund et al. (1993), Kritzer and Goldman-Rakic (1995), Puckak et al. (1996) and Malach et al. (1997)
	Prefrontal			Lewis et al. (2002)
	Inferotemporal (IT) area TE	0.45–0.51	0.7–1.3	Levitt et al. (1994) and Tanigawa et al. (2005)
	Inferotemporal (IT) area TEO	0.42	0.7	Levitt et al. (1994)
	Motor (forelimb representation)	0.375–1	0.75–2	Huntley and Jones (1991)
	Area V1	0.15–0.32	0.4–0.75	Fisken et al. (1975), Rockland and Lund (1983), Livingstone and Hubel (1984b), Yoshioka et al. (1992), Amir et al. (1993), Lund et al. (1994), Malach et al. (1993), Coogan and Van Essen (1996), Yoshioka et al. (1996), Angelucci, Levitt, Walton, et al. (2002), Stettler et al. (2002), and Tanigawa et al. (2005)
	Area V2	0.25–0.4	0.6–0.7	Rockland (1985a), Yoshioka et al. (1992), Amir et al. (1993), Lund et al. (1993), and Coogan and Van Essen 1996
	Area V4	0.27–0.35	0.6–0.92	Yoshioka et al. (1992), Amir et al. (1993), and Lund et al. (1993)
Owl monkey	Area MT	0.33	0.827	Malach et al. (1997)
Galago	Area V1			Cusick and Kaas (1988b)
Quokka	Area V1	0.32	0.548	Tyler et al. (1998)
Squirrel monkey	Area V1	0.2	0.4	Rockland and Lund (1983) and Sincich and Blasdel (2001)
	Area V2	0.2–0.27	0.62–0.7	Livingstone and Hubel (1984a), Rockland (1985a), Cusick and Kaas (1988a), and Malach et al. (1994)
	Area DL_C (V4)	0.29	0.58	Cusick and Kaas (1988a) and Weller et al. (2000)
	Area DL_R			Cusick and Kaas (1988a)
	Areas 3b and 4	0.75	1.5	Jones and Wise (1977)
Human	Area V1	0.3–0.5	0.6–1.0	Burkhalter and Bernardo (1989)
	Area V2	0.3–0.5		Burkhalter and Bernardo (1989)
	Area 22	0.56–0.86	1.02–1.63	Galuske et al. (2000)
	Area 41 (A1)	0.39–0.42	0.87–0.95	Galuske et al. (2000)
Tree shrew	Area 17	0.23–0.33 mm	0.48–0.5 mm	Rockland et al. (1982), Rockland and Lund (1982), Sesma et al. (1984), and Bosking et al. (1997)

Note: References are listed where punctate labeling of intrinsic projections was observed following tangential sectioning or reconstruction of cortical tissue, labeled with various anterograde, retrograde and bidirectional tracers. Values reported here are ranges of reported means, not minima and maxima. Measurements are as reported in the original work, except those marked with , which were estimated by us from the published material. Although a single rodent is included in this table, the presence of a patch system in the rodent is controversial—for a discussion, see Muir and Douglas (2010).

patch system in shaping the cortical response. We propose that the superficial patch system is an anatomical substrate encoding a statistical expectation of the cortical response. This fact becomes easily observable for a particular class of stimuli; specifically, stimuli that require encoding of identical stimulus parameters over the full extent of the visual field. The cortical response to these stimuli consists of active regions that collectively encode identical functional parameters. We call these evoked cortical states "self-consistent" states, since each active region encodes parameters of the stimulus that are consistent with all other concurrently active regions across the visual cortex. Comparisons between the patch system and the cortical response made using aggregate maps of function, such as angle maps of orientation preference, may obscure the relationship between self-consistent states and the patch system. Here, we directly search for evidence linking the patch system and self-consistent cortical states by comparing their respective spatial arrangements.

Although "superficial" is the most common epithet ascribed to the patch system, a similar and underexplored pattern of clustered labeling exists in layers 4 and 5 (Asi et al. 1996; Lund et al. 2003; Shmuel et al. 2005; Angelucci and Sainsbury 2006). We have restricted ourselves to examining the patch system in the superficial layers due to the availability of functional imaging in these layers, as well as the relative paucity of data from deeper cortical layers (but see Karube and Kisvárday 2010).

Materials and Methods

Briefly, we recorded functional maps from cat and macaque monkey primary visual cortex (area 17 only, in both species), representing the cortical response to high contrast, full-field drifting square-wave grating stimuli. We recorded blank-subtracted single-condition maps (response maps) using optical imaging (OI) of the intrinsic signal (cats) and voltage-sensitive dye imaging (cats and monkeys). Response maps had a punctate appearance, where restricted regions of cortex were activated by the visual stimulus (active regions). A series of image processing steps were applied to each response map to locate the centers of active regions. Gabriel graphs, which define adjacency

relationships over a set of points (Gabriel and Sokal 1969), were used to identify neighboring active regions over each response map.

Our measurements of the spatial configuration of the superficial patch system were made over a database of figures showing patchy labeling following injections into primary visual cortex of the cat and macaque monkey, collected from the last 28 years of literature. We manually annotated these figures with the locations of labeled patches and used Gabriel graphing to construct neighbor graphs as for the OI response maps. The full list of patch-labeling injections used in this work is given in Supplementary Tables 1–2.

We measured the distributions of interior angles formed by the neighbor graphs of OI response maps and sets of patches labeled by single injections of neural tracer (patch spreads). The distribution of interneighbor angles is a measure for lattice structure in a graph, if present, and can distinguish between random arrangements and between various regular and noisy lattice structures. We compared the distributions of angles against distributions formed by random models, namely hexagonal and square lattices with various amount of jitter. Our analysis is illustrated in detail in Supplementary Figures 1–3, with examples from 3 patch-labeling injections.

Our data collection and analysis were restricted to area 17 (primary visual cortex) of the cat and macaque monkey. Where we refer to "primary visual cortex" in the text, we mean only area 17; likewise, where we use the term "monkey" to refer to our results we mean only macaque monkey. The remainder of this methods section describes in detail the data collection and analysis techniques outlined above.

Macaque and cat voltage sensitive dye imaging experiments and surgical procedures were performed in the lab of A. Grinvald, according to the NIH guidelines under protocols approved by the animal care committee of the Weizmann Institute of Science. Experimental protocols for intrinsic optical imaging of cat visual cortex were approved by the Kantonal Veterinaeramt of Zurich, and performed under licenses 50/2003 and 164/2006 granted to K.A.C. Martin for the project "Microcircuits of Neocortex."

Surgery and Imaging

Adult and juvenile (9 weeks old) cats were anesthetized and sedated before surgery with an initial dose of 0.6 mL ketamine (Narketan) and 0.15 mL xylazine (Rompun), then anesthetized during surgery with halothane (0.5–2.0%) in a 1:1 mixture of N_2O and O_2, and with alfaxolone 9 mg/mL and alfadolone 3 mg/mL (Saffan), delivered intravenously 1:2 in saline as required. A femoral intravenous cannula was inserted, through which anesthetic and paralysant were administered throughout the course of the experiment. The femoral artery was also cannulated to measure blood pressure over the course of the experiment. Animals were artificially respirated either through an orotracheal tube or tracheotomy, and the animal was mounted in a stereotaxic frame.

Halothane anesthetic delivery was reduced to 0.25% (and as required), and the N_2O/O_2 mixture was changed to 2:1. Animals were paralyzed with an initial dose of 40 mg gallamine triethiodide (Sigma) in 8 mL of saline, then placed on continuous pump delivery of 0.75 mg/mL tubocurarine chloride hydrate (Sigma) and 8 mg/mL gallamine triethiodide (Sigma) in saline (2.6 mL/h). Anesthesia was maintained by pump delivery of Saffan 1:2 in saline (1.2 mL/h); electroencephalography (EEG), electrocardiogram, blood pressure, and heart rate were monitored, and anesthetic delivery was adjusted as necessary to maintain the level of anesthesia, as judged by the presence of a "spindling" EEG trace. Body temperature was maintained with a thermostatically controlled heating blanket, and end-tidal CO_2 was maintained between 4.4 and 4.6%.

Nictitating membranes were retracted with phenylephrine drops, pupils were dilated with atropin drops (1%), and gas permeable contact lenses inserted to prevent dehydration of the cornea. A high-contrast CRT stimulus screen (Sony) was placed 57 cm from the animal. The eyes were refracted and corrective lenses used to focus the eyes on the screen. The projection of the fundus on the stimulus screen was ascertained to ensure that stimuli were presented in the central visual field.

Craniotomies were made in both hemispheres over the central visual field representation in area 17 (primary visual cortex). Craniotomies revealed regions of cortex up to 3 × 6 mm in size around the area centralis representation, corresponding to approximately 5 × 10° of the visual field (Tusa et al. 1978). A metal chamber was cemented to the skull over the craniotomy, filled with silicone oil and sealed with a transparent glass cover slip. In most animals, the dura was reflected and the cortex imaged directly. In some experiments, imaging was attempted through the dura. In cases, where response maps could not be obtained with this method, the dura was reflected and the cortex imaged directly.

Optical imaging of the intrinsic signal associated with cortical activity was performed using a technique similar to those of Grinvald and colleagues (Grinvald et al. 1986; Bonhoeffer and Grinvald 1991). After obtaining an image of the cortical vasculature and extent of the craniotomy under green illumination, the focal plane was lowered to 450 μm below the pial surface. Visual stimuli were generated by a computer running custom software written in Matlab (The Mathworks). Square-wave gratings of high contrast (1 cycles/degree, drifting at 1 cycle/s, covering 40° of the visual field) were presented at either 8 or 16 equally spaced orientations and oscillating along an axis orthogonal to that of the grating bars. Images of the intrinsic signal were obtained under illumination with orange (600 ± 5 nm wavelength) light, using an Imager 3001 system (Optical Imaging, Inc.) with reverse-coupled 50 mm (f 1.2) and 135 mm (f 2.0) lenses and a Dalsa 1M60 CCD camera (1024 × 1024 frame size). Stimuli were presented in random order, in blocks spanning the full range of orientations used, plus a blank stimulus. During a prestimulus interval of 7 s, a fixed grating of a given orientation was displayed. During the following 3 s, the grating oscillated as described above, and recording of the optical signal from cortex took place. Presenting the upcoming stimulus during the prestimulus period avoids a transient nonspecific cortical response due to the stimulus being flashed on the screen. Five frames were collected over the recording period, of which the last 4 were selected for further analysis, excluding the "initial dip" portion of the cortical response.

Surgery and voltage-sensitive dye imaging methods for awake behaving macaque monkeys are described in detail in Grinvald et al. (1991), Shtoyerman et al. (2000), and Slovin et al. (2002). Briefly, macaque monkeys 6 years of age were trained to view a video monitor. Under general anesthesia, titanium screws were implanted in the skull for head restraint, and an optical chamber covering primary visual cortex (area 17; V1) was mounted on the skull with dental cement. A thin, transparent silicone artificial dura with infusion tubes was implanted over the exposed cortex. At the start of each recording session, oxonol voltage-sensitive dyes were infused over a period of 2 h. Animals fixated on a small dot while high-contrast square-wave gratings (2 cycles/degree, shifting at 2 cycles/s, 4 orientations) were presented on a monitor placed 100 cm from the animal and covering approximately 13 × 13° of the visual field. Response frames of 60 × 60 pixels were collected at 100 Hz, covering an area of 3.6 × 3.6 mm (60 μm interpixel resolution).

Frames recorded in response to a single-orientated stimulus were summed together, and the recorded cortical response to nonstimulus (blank) conditions was subtracted to obtain a map of the differential response to a single orientation (called an OI response map in this report). Divisive or subtractive normalization of orthogonal orientation response maps was not performed.

Location of Active Regions on OI Response Maps

We applied a series of image processing techniques to OI response maps to enhance their signal-to-noise ratio, and then located the centers of active regions using a model of a region of neural activity. This process is illustrated in Figure 1. A single-condition OI response map is an image $\boldsymbol{R}: \mathbb{R}^2 \rightarrow \mathbb{R}$. We defined positions in map space $\mathbf{u}, \mathbf{v} \in \mathbb{R}^2$. For each experiment, we formed a mask excluding regions of the imaging area covered by the skull, or by cortical vasculature, from analysis. These masks have the form:

$$M(\mathbf{u}) = \begin{cases} 1, \text{for valid regions of analysis} \\ 0, \text{otherwise} \end{cases}. \quad (1)$$

We consider that $M(\mathbf{u})$ is zero for regions completely outside the imaging area. Our model for an active region had the form of an isotropic Gaussian field, that is,

$$\mathcal{G}(\mathbf{u},\mathbf{v},\sigma_D)=\frac{\exp\frac{-\|\mathbf{u},\mathbf{v}\|^2}{2\sigma_D^2}}{2\pi\sigma_D^2}, \quad (2)$$

where $\|\mathbf{u},\mathbf{v}\|$ is the Euclidean distance between the field center $\mathbf{u}$ and an arbitrary point $\mathbf{v}$. We took the width of an active region as 4 standard deviations, containing approximately 98% of the weight of the Gaussian field. Our active region models had a width of 600 μm for the cat (i.e., σ_D = 150 μm) and a width of 400 μm for the macaque monkey (i.e., σ_D = 100 μm). These values were chosen empirically to approximate the average size of active regions in our OI response maps.

Low-frequency variations in OI response maps were removed by subtracting the local average of a single map. The local average of a map $\boldsymbol{R}$ was calculated by convolution with a disk kernel D_r, where

$$\mathcal{D}_r(\mathbf{u})=\begin{cases}1, \|\mathbf{u}\|\leq r\\ 0, \text{otherwise}\end{cases}, \quad (3)$$

and $\boldsymbol{r}$ is the radius of the disk kernel. The local average subtracted map $\hat{R}$ is then given by

$$\hat{R}=R-R\otimes\mathcal{D}_r. \quad (4)$$

In this work, we used a disk kernel with a diameter 3 times that of the active region model.

OI response maps were then thresholded to the mean response of the area within a mask defined by the visible region inside a craniotomy; that is,

$$\bar{R}(\mathbf{u})\begin{cases}\max(\hat{R},\langle\hat{R}\rangle_M), & M(\mathbf{u})=1\\ \langle\hat{R}\rangle_M, \text{otherwise}\end{cases}. \quad (5)$$

Here $\langle\hat{R}\rangle_M$ is the spatial average of a response map, computed for regions within the mask M using the expression:

$$\langle\hat{R}\rangle_M=\frac{1}{\sum_{\mathbf{u}}M(\mathbf{u})}\cdot\sum_{\mathbf{u}}[M(\mathbf{u})\cdot R(\mathbf{u})]. \quad (6)$$

We calculated the cross-correlation of the Gaussian field model with a response map to emphasize locations on the response map that corresponded to the centers of active regions. We used the normalized fast cross-correlation measure of Lewis (1995), namely

$$\gamma(R,\mathcal{G}_{\sigma_D},\mathbf{u})=\frac{\sum_{\mathbf{v}}(R(\mathbf{v})-\langle R\rangle)(\mathcal{G}(\mathbf{u},\mathbf{v},\sigma_D)-\langle\mathcal{G}(*,*,\sigma_D)\rangle)}{\sqrt{\sum_{\mathbf{v}}(R(\mathbf{v})-\langle R\rangle)^2\cdot\sum_{\mathbf{v}}(\mathcal{G}(\mathbf{u},\mathbf{v},\sigma_D)-\langle\mathcal{G}(*,*,\sigma_D)\rangle)^2}}. \quad (7)$$

Here $\langle R\rangle$ is the spatial average of a response map $\boldsymbol{R}$ and $\langle\mathcal{G}(*,*,\sigma_D)\rangle$ is the spatial average of the Gaussian kernel with standard deviation σ_D. $\gamma(R,\mathcal{G}_{\sigma_D},\mathbf{u})$ is a mapping $\gamma:\mathbb{R}^2\rightarrow\mathbb{R}$ defined over the same region of space as $\boldsymbol{R}$, for which the value of at the position $\mathbf{u}$ gives the coefficient for the correlation of $\boldsymbol{R}$ and the Gaussian kernel centered at $\mathbf{u}$.

Positions in space that had a correlation with the Gaussian model of less than 10% were excluded from further analysis by augmenting the mask $\boldsymbol{M}$:

$$M'(\mathbf{u})=\begin{cases}1, (M(\mathbf{u})=1)\wedge(\gamma(\bar{R},\mathcal{G}_{\sigma_D},\mathbf{u})\geqslant 0.1)\\ 0, \text{otherwise}\end{cases}. \quad (8)$$

The matrix composed of correlation coefficients was processed with nonmaximum suppression to identify the points in the original OI response map that corresponded to the centers of active regions. This was accomplished by performing a morphological dilation of γ with a disk kernel D_r that has the same diameter as the active region model. The centers of active regions were identified as those points for which the morphological dilation did not change the value at that point, that is, we define the set:

$$A:\left[\begin{array}{l}\text{dilate}(\gamma(\bar{R},\mathcal{G}_{\sigma_D},\mathbf{a}_i),\mathcal{D}_r,\mathbf{a}_i)=\gamma(\bar{R},\mathcal{G}_{\sigma_D},\mathbf{a}_i)\\ \|\mathbf{a}_i,M'(\mathbf{u})\|\geqslant d, M'(\mathbf{u})=0\end{array}\right]\rightarrow\mathbf{a}_i\in A. \quad (9)$$

Here, $\text{dilate}(O,K,\mathbf{u})$ is the value of the morphological dilation of matrix $\boldsymbol{O}$ with kernel $\boldsymbol{K}$ at a location $\mathbf{u}$. The second condition for inclusion in $\boldsymbol{A}$, given in equation (9), excludes points closer than a distance $\boldsymbol{d}$ to the edge of the craniotomy mask M'. We excluded points closer than half of the Gaussian model width to craniotomy mask; this prevented identification of spurious centers, caused by reflections from the craniotomy edge or by other artifacts, for example, those caused by the curvature or vascular architecture of the cortex.

Identification of Neighbors

A Gabriel graph was constructed to identify neighboring active regions on a single-condition map. Figure 2 illustrates the result of this process,

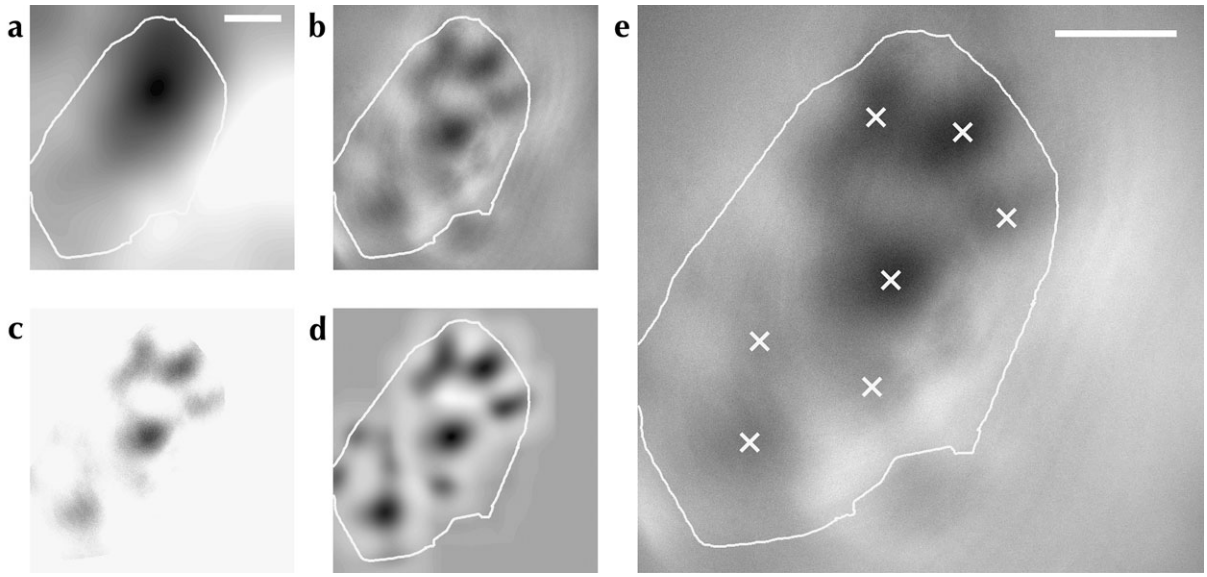

Figure 1. Active region location process shown for a single OI response map. The local average (shown in *a*) of the response map was obtained by convolution with a disc kernel. This result was subtracted from the response map to remove large-scale variations in the image (*b*). The map was then thresholded to the mean of the area within the craniotomy mask (shown as a white outline on all subfigures); the result is shown in *c*. A Gaussian field was used as a model of an active region, and the correlation between this model and all points on the map was calculated (*d*). This results in a smooth image where peaks of higher intensity indicate the position of activity bumps in the original map. Peak locations were identified using nonmaximum suppression; these locations are shown in *e* as white crosses on the original OI response map. Scale bars: 1 mm.

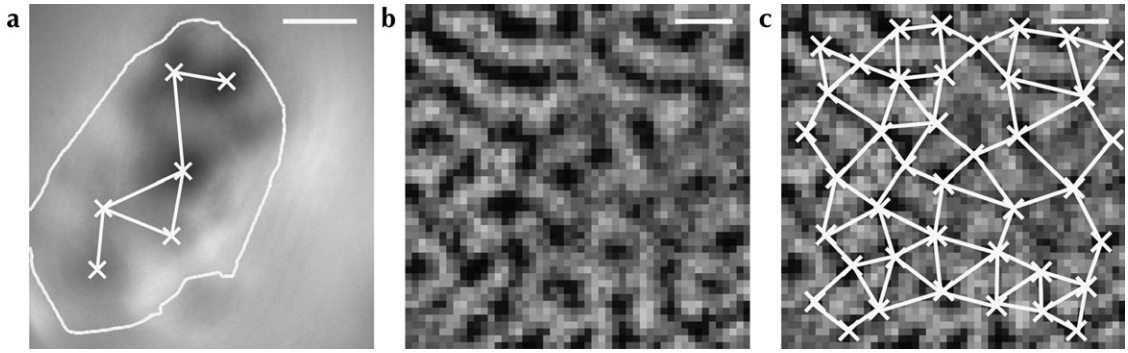

Figure 2. Neighborhood relationships between active orientation-responsive regions across visual cortex. (*a*) The same OI response map from cat primary visual cortex as shown in Figure 1, with the corresponding neighborhood graph superimposed. Neighbor relationships (white lines) between the active regions (crosses) were calculated using Gabriel graphing (Gabriel and Sokal 1969). The existence of an edge between 2 points on the graph indicates that these points are considered to be neighbors. Only connected vertices are shown. (*b*) An example functional map from monkey area V1 used in our analysis. (*c*) The functional map from (*b*), with the identified active regions (crosses) and corresponding neighborhood graph (white lines) superimposed. Scale bars: 1 mm.

with further examples for patch-labeling injections given in Figure 6 and Supplementary Figures 1–3. Gabriel graphs define neighbor relationships between a set of points over space (Gabriel and Sokal 1969). Two points **a** and **b** are neighbors if and only if all other points in the set are outside the circle on whose circumference **a** and **b** are at opposite points, known as the "neighborhood circle." We extended this definition to exclude pairs for which the neighborhood circle intersected either the edge of the craniotomy mask or the edge of the OI response map. This criterion was used because another peak could have existed just off the edge of the visible region of cortex but still within the neighborhood circle. If such a peak existed, it would exclude the 2 points under consideration from being accepted as neighbors. Marking them as neighbors might distort the distribution by introducing relationships that are merely artifacts of the shape of the craniotomy.

Neighborhood graphs produced in this way are unique and are defined only by the spatial configuration of vertices in a graph. A single vertex may have any number of neighbors or none—the neighborhood criteria are not restricted to produce a triangulation, for example.

Characteristic Measures

Several spatial measurements were taken in order to examine the structure of the neighborhood graphs formed by configurations of active regions and of labeled patches (summarized in Fig. 3). Interpoint distances were collected between pairs of vertices meeting the neighborhood criteria to measure spatial scale. The angles formed by edges drawn between sets of neighboring vertices were also collected, for vertices with at least 2 neighbors. The distribution of these angles gives a density-free measure of statistical shape over our neighborhood graphs. Our approach is similar to that of Boots, who defined a technique for the statistical analysis of shape based on the interior angles of Delaunay triangles defined over a set of points (Boots 1974). Shapiro et al. (1985) used a similar method, building the Voronoi cells (the dual of the Delaunay graph) and measuring the angles formed between Voronoi cell centers and the vertices of the same cell. We use the same measure of shape as Boots, with the exception of our use of Gabriel graphing to form lines between neighboring points.

We measured interior angles around a single vertex by taking acute angles formed by adjacent neighbor edges. If a pair of vertices were rejected as being neighbors due to their proximity to the edge of the map, then angles formed by this pair of vertices at a third vertex were discarded. These criteria and the interneighbor angle collection method are illustrated in Figure 3. We estimated the variance of these measures by performing a bootstrap analysis (Efron 1979) over sets of functional maps grouped by experiment and subsequently estimating confidence intervals (CIs) for the measured distributions. Comparisons between sets of angular distributions were made using the 2-sided Kolmogorov–Smirnov (K–S) test, which determines whether 2 sample sets have been drawn from the same distribution (Kolmogorov 1933; Smirnov 1939; Massey 1951). A value for P below the threshold for significance indicates that we must reject the null hypothesis that the distributions are equivalent. Note that this test makes no assumptions about the shape of these distributions; in particular, it does not require the data to be normally distributed.

The advantage conferred by this technique is that we can distinguish not only between Poisson, regular and clustered distributions but also examine any lattice regularities that may underlie the spatial arrangement of points. An example showing distributions based on square and hexagonal lattices is illustrated in Figure 5. A kernel density method was used to visualise the distributions presented in figures 8–12. Gaussian kernels with widths of 8 degrees (for angle distributions) and 100 μm (for distance distributions) were convolved with each observation. This technique was used only for visualisation, and not for comparing distributions.

Database of Patch-Labeling Injection Experiments

We assembled a database of 374 figures illustrating injections into the superficial layers of cortex from a large selection of the patch-labeling literature, covering predominately cat, old- and new-world monkeys, and tree shrew. In this paper, we restricted ourselves to reconstructions of injections revealing the patch system over reasonably large areas of primary visual cortex (area 17–V1) in cat and macaque monkey. Most neural tracers are not restricted to unidirectional tracer transport, especially when large pressure injections are made. For this reason, no attempt was made to distinguish between anterograde and retrograde labeling, unless pure anterograde or retrograde labeling was reported in the source material. Following the frequent observation of patches containing colocated anterogradely and retrogradely labeled material (Rockland et al. 1982; Rockland and Lund 1983; Tyler et al. 1998; Angelucci, Levitt, Lund, et al. 2002), we assumed that the spatial statistics of the superficial patch system was independent of the directionality of the tracer used.

The wide assortment of tracers and variety of injection techniques leads to a wide variation in the sizes of injection sites, the intensity of labeling, and the number of labeled neurons. We assumed that an increase in the number of labeled patches or labeled neurons did not change the spatial statistics of the superficial patch system or the spatial arrangement of patches. Reconstructions showing abutting or overlapping patches were excluded from analysis, as we could not unambiguously identify patch centers in these cases. Also excluded were cases where injections were not confined to area 17 or where injections had been made into several cortical areas. This reduced our data set to 13 injections made into cat area 17 and 27 injections made into V1 of macaque monkey (for references, see Supplementary Tables 1–2). An example annotated figure from our database is shown in Figure 6; this injection was reported in Tanigawa et al. (2005). The steps taken in our analysis are illustrated in detail for 3 patch system injections in Supplementary Figures 1–3. The full list of patch-labeling injections used for analysis in this report is given in Supplementary Tables 1–2.

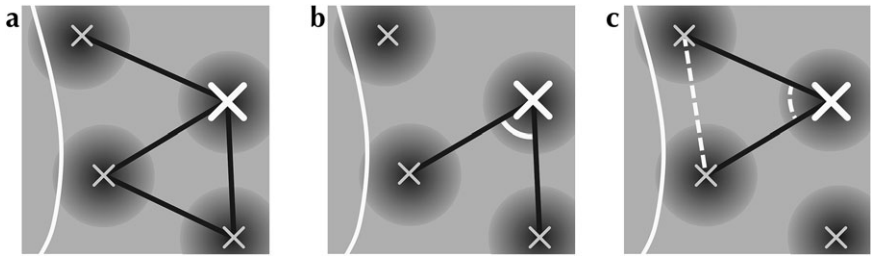

Figure 3. A schematic illustration of how angles between neighbors are measured. Active regions are indicated with crosses over a portion of a cartoon orientation map (*a*). For the equivalent analysis of patch-labeling experiments, crosses would indicate the centers of identified patches. Neighbor relationships between vertices are shown as solid lines connecting neighboring crosses. The edge of the craniotomy mask is shown as a thick white line. The large cross is the vertex for which interneighbor angles will be collected. *b* shows an angle that meets the criteria for measurement. The white arc indicates the pair of neighbor relationships that define this angle at the vertex under analysis. Note that in all cases only the acute angle is measured, and the complementary obtuse angle is ignored. *c* shows an angle that does not meet the criteria for measurement. In this case, the secondary neighbor relationship that would connect the 2 primary neighbors is missing (indicated by a dashed line); the neighborhood circle for these 2 points intersects the edge of the craniotomy (see Materials and Methods).

Artificial Models of Spatial Arrangement

Uniform Random Model

Artificial models of active regions on OI response maps and of patch locations resulting from injections were used to compare the respective spatial distributions of cortical function and anatomy against several types of random distribution. The first such model comprised locations drawn from a Poisson distribution within a craniotomy mask (for comparison with OI response maps) or within the region spanning a set of labeled patches (for comparison with the reconstructed anatomy). The number of locations used in each artificial map or patch spread followed the distribution of the number of active regions and labeled patches in our source data. Neighborhood relationships between artificial locations were identified in the same manner as described previously for the OI response maps and for patch spreads.

Lattice Models

We used a generalized Neyman–Scott process (Neyman and Scott 1958) to design several models of spatial arrangement with predefined lattice structure (examples shown in Fig. 4). Seed points were drawn from a perfect hexagonal or square lattice, with uniform random origin and orientation, and a spacing equal to the average distance between neighboring active regions (for comparison with functional maps) or between neighboring patches (for comparison with patch-labeling injections). A single secondary point was generated close to each seed point by drawing from a uniform random distribution centered at that seed point. These secondary points were used as the locations of synthetic active regions or synthetic patches. The maximum distance from a secondary point to its seed point was some factor δ of the nominal grid distance; a value of $\delta = 0$ results in a set of points with perfect lattice structure (but quantized to discrete pixel locations). A value of $\delta = 1$ defines a model, where each point is moved up to a distance of the nominal lattice spacing from its seed point. As δ increases, the distribution of points changes from a perfect lattice structure to a Poisson process. Neighborhood relationships between peaks were identified in the manner described in Characteristic Measures.

For each artificial model, we generated the same number of maps and injections as we obtained experimentally, covering the same area of cortex, using the experimentally obtained craniotomy and patch masks and with the same density of active regions as measured from the OI response maps and from the patch spread reconstructions. In this way, we neutralized the unquantifiable edge effects introduced into our measured distributions by the irregular craniotomy shapes produced by the imaging experiments. We estimated the variance of these artificial models by generating several random sets of synthetic active region and patch locations.

Figure 5 shows a step-wise variation between perfect lattice structure and no structure for both the hexagonal and the square models. Perfect lattices produce measured angle distributions with strong peaks at the angles that follow from the underlying lattice structure (i.e., 60° for the model with hexagonal structure; 45° and 90° for the square model). Since we restrict points to fall on discrete pixel locations, a model with zero jitter will not produce the delta-width spike at the signature angles that would be expected from a perfect lattice. Nevertheless, by using our criteria for identifying neighbors and performing the measurement of angles as we describe above, we can clearly distinguish between Poisson systems and systems with regular structure, while also collecting evidence for a particular order of lattice angular symmetry. Note the bimodal distribution of angles in Figure 5*b*. This occurs as δ increases for the square model, increasing the chance of identifying as neighbors 2 diagonally opposite points in the square lattice and consequently increasing the proportion of 45° angles observed in the distribution.

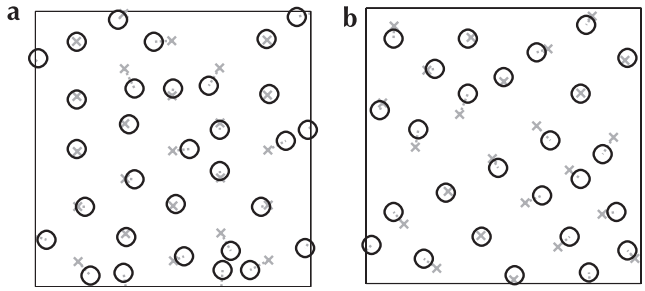

Figure 4. Examples of jittered lattices, generated through a Neyman–Scott process (Neyman and Scott 1958). Base grids following a perfect hexagonal (*a*) or square (*b*) lattice are generated with random origins and rotations (gray crosses). For each vertex of a base grid, a secondary point is generated, at a uniform random offset from the base vertex (up to a factor δ of the nominal grid spacing) and with a uniform random offset direction (black circles). These secondary points are used as artificial patch or active region locations in our analysis. In this figure a jitter of $\delta = 0.5$ is illustrated, which was the amount of jitter we found to most closely reproduce the measured experimental spatial distributions. The distributions of intervertex angles produced by these models are shown in Figure 5.

Comparison between Patch-Labeling Injections and OI Response Maps

Our characteristic measures are sensitive to the shape of the outline of a given set of points. For our artificial lattice models, we corrected for this source of error by masking each set of generated points with an experimentally obtained craniotomy outline. Performing this correction becomes more difficult when we compare a group of patches resulting from an injection with an OI response map, since both data sets have irregular borders. In cat area 17, patch spreads are often larger in extent than the region of visual cortex available for functional imaging. Monkey V1 provides a greater surface for imaging, as well as a higher density of active regions of cortex in each map, which allowed us to subsample the imaging data.

We corrected for these edge effects by taking the convex hull of a patch spread resulting from a single injection, then using this as a mask over a single OI response map. We placed this mask with random position and orientation to fit inside a response map and extracted the centers of active regions that fell within the mask. In this way, we resampled our functional maps to impose the same bounding shapes that were present in our patch-labeling data set. This process is illustrated in Figure 6.

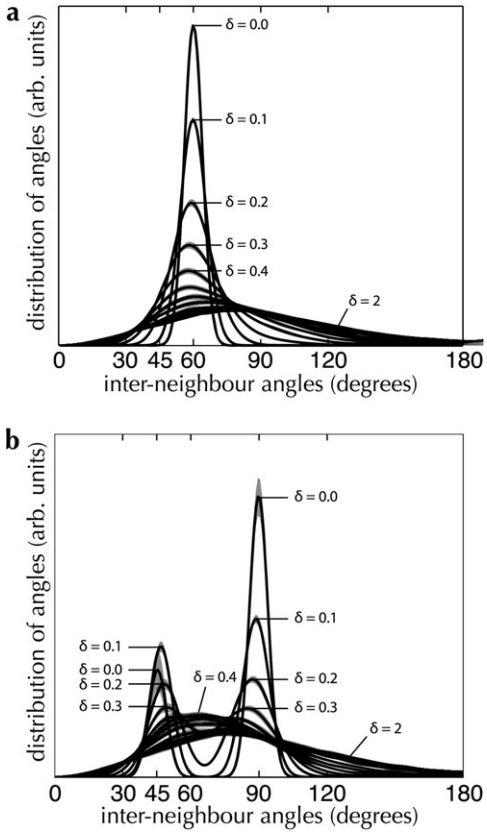

Figure 5. Interneighbor angle distributions for 2 regular lattice models. Point sets were generated from lattice models with underlying hexagonal (*a*) and square (*b*) structures, as described in Materials and Methods. In both graphs, the degree of jitter (δ) is varied between 0 (a perfect lattice) and 2 (close to a Poisson distribution). Dark lines indicate the mean distribution; shading indicates the 95% CI, estimated over 100 random instances for the same jitter parameter.

Results

Cross-Species Examination of the Superficial Patch System

We collected observations of clustered labeling following injections of neural tracer from published literature (see Table 1). Reconstructed sets of patches labeled by single injections of tracer (patch spreads) were included when the reconstructions had been made from tangentially sectioned tissue or when large tangential-view reconstructions had been made from multiple nontangential serial sections. We observed a simple scaling rule followed by the superficial patch system across species and across cortical areas: the spacing between neighboring-labeled patches is approximately double the width of a single patch (see Fig. 7).

We assembled a database of figures from published papers showing the results of patch-labeling experiments spanning the last 28 years. Without access to the original material and to obviate the need for arbitrary and highly subjective assumptions about where to draw patch boundaries, we included only figures showing reconstructions of photomicrographs, under the assumption that the original researchers knew best what they were looking at. Patch locations were identified by the original researchers; we extracted the centers of patches either directly (when marked on the reconstructions) or by taking the center of mass of each outlined patch. An example annotated figure from our database is shown in Figure 6*a*, and the full analysis technique is illustrated in detail in Supplementary Figures 1–3. The full list of figures used in our analysis is given in Supplementary Tables 1–2.

We recorded single-condition OI response maps indicating orientation preference across the surface of area 17 in adult cats and macaque monkeys. A total of 266 response maps were obtained from 19 cats; 2 monkeys were used for a total of 16 response maps. Details of these experiments and the animals used are listed in Tables 2 and 3.

Spatial Characteristics of Patch-Labeling Injections and OI Response Maps

Our measurements of the spatial distributions of labeled patches and active regions in area 17 of cat and macaque monkey are summarized in Table 4. The shape of our measured distributions for interneighbor angles is highly skewed (see Figs 8 and 9), as are the expected distributions for our artificial models of patch and active region locations shown in Figure 5.

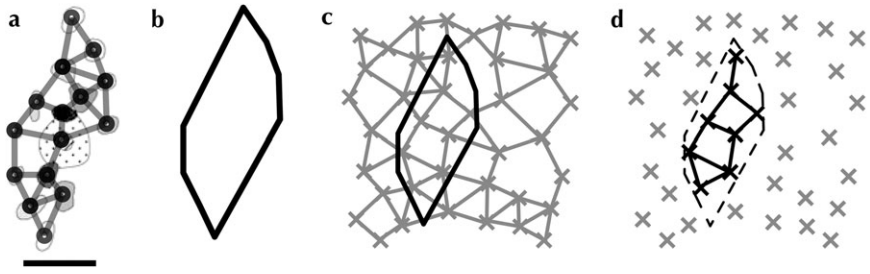

Figure 6. Illustration of the resampling process used to compare patch-labeling injections with OI response maps. An example injection reconstruction from our database is shown in *a*. An injection of biotinylated dextran amine (central hashed region) was made into macaque monkey V1 by Tanigawa and colleagues (reproduced with permission from Tanigawa et al. 2005; scale bar: 1 mm). We located the center of the reconstructed patches and identified the neighborhood graph as described above (black circles and connecting lines). We constructed the convex hull of the labeled patches (*b*), then superimposed this hull onto a set of active regions identified from an OI response map (*c*). Using the hull as a mask, we excluded active regions and neighbor relations falling outside this region (gray crosses: *d*). In this way, we imposed the shape of a patch group onto the structure of an OI response map, ensuring that any potential distortions in our characteristic measures caused by the shape of a set of points were included equally in both data sets. The points and neighbor relations that remained after masking were used to compare the spatial arrangement of the OI response maps with that of the patch-labeling injections.

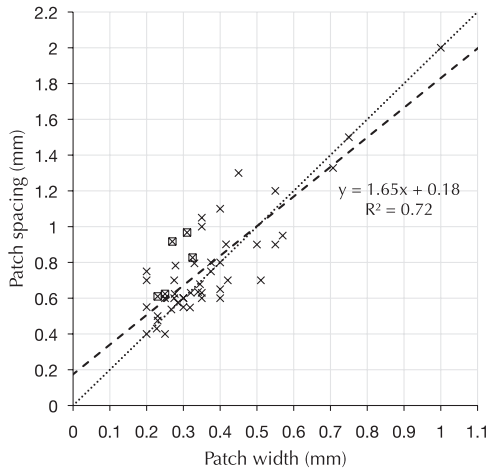

Figure 7. Patch spacing versus patch width across many species and cortical areas. Observations of clustered labeling from Table 1 are shown here, when data for both patch width and patch spacing were reported. Each × is an individual observation of clustered labeling of intrinsic projections in a cortical area. A boxed × indicates that we have estimated the value of patch spacing from the published material. The dashed line is a linear regression of the data shown here, and explains 72% of the observed variance. The dotted line has a slope of 2 and is provided for comparison.

Table 2
List of imaging experiments performed to collect OI response maps form cat primary visual cortex

Animal identifier	Age	Number of stimuli (number of maps)	Imaging technique
2303	9 weeks	8 (16)	Intrinsic signal
2403	9 weeks	8 (8)	
0806	37 weeks	8 (8)	
1206	45 weeks	8 (21)	
1306	48 weeks	8 (8)	
1606	56 weeks	16 (16)	
1906	57 weeks	16 (16)	
2006	57 weeks	16 (80)	
2506	67 weeks	8 (8)	
2806	2 years	8 (8)	
1207	21 weeks	8 (8)	
0208	37 weeks	8 (8)	
0408	2 years	8 (8)	
0508	62 weeks	8 (8)	
01apr03	8 months	6 (6)	Voltage-sensitive dye
15dec04	12 months	4 (4)	
21dec04	10 months	4 (4)	
19apr05	11 months	6 (6)	
07may07	12 months	6 (6)	

Note: The "Animal identifier" column lists our identifying code for a particular animal. "Number of stimuli" indicates the number of different orientations that were used for collecting OI response maps. In several cases (animals 2303, 1206, 1606, 1906, and 2006), more than one recording session was used for analysis. The total number of single-condition maps collected for an animal is indicated in brackets. The exact age in weeks was not available for animals 2806 and 0408. "Imaging technique" lists the type of imaging used to record the cortical response. Area 17 (primary visual cortex) was imaged in all animals.

Table 3
List of imaging experiments performed in macaque monkey primary visual cortex

Animal identifier	Age (years)	Number of stimuli (number of maps)	Imaging technique
3	6	4 (12)	Voltage-sensitive dye
4	6	4 (4)	

Note: Column names have the same meaning as in Table 2. Area V1 (primary visual cortex) was imaged in all animals.

Although the distributions of interneighbor distance are closer to being normally distributed, they are skewed enough that for all distributions we report the mode and its CI. Means for distances are reported in Table 4 and below.

The distance between labeled patches was 0.90 [0.81–1.03] mm and 0.50 [0.41–0.59] mm for cat and monkey, respectively (N.B. mode [95% CI]). The distance between active regions was 1.01 [0.95–1.07] mm and 0.74 [0.71–0.77] mm for cat and monkey, respectively. In the cat, a physical displacement of around 1 mm across area 17, close to the area centralis, corresponds to approximately 1 visual degree of displacement—a value known as the cortical magnification factor (Tusa et al. 1978). Our measurements of interpatch and interdomain spacing for the cat then also correspond to around 1 visual degree, on average. In macaque monkeys, the cortical magnification factor varies between around 1 and 3 mm/degree close to the central visual representation, with a differential magnification favoring the vertical meridian for which we did not correct (Van Essen et al. 1984). In macaque area V1, we measured interpatch distances corresponding to approximately 0.17–0.5 visual degrees and interdomain distances corresponding to 0.25–0.74 visual degrees.

Our measurements of interpatch and interdomain spacing are consistent with previous reports of mean spacings. We estimated the average distance between active regions in cat area 17 at 1.05 mm, within the reported range of means of 1–1.14 mm (Albus and Sieber 1984; Diao et al. 1990; Hübener et al. 1997; Rao et al. 1997). In the monkey, our measurement of 740 μm for mean interdomain spacing is within the reported range of 640–760 μm (Stettler et al. 2002; Lund et al. 2003). Our estimate of mean interpatch spacing in the cat of 1.06 mm is within the reported range of 1.05–1.1 mm (Luhmann et al. 1990; Kisvárday and Eysel 1992); our measured mean interpatch spacing in the monkey of 520 μm is within the reported range for means of 450–750 μm (400 μm, 425–450 μm, 450–500 μm, 500–600 μm, 610 μm, and 750 μm; Rockland and Lund 1983; Yoshioka et al. 1992; Amir et al. 1993; Tyler et al. 1998; Angelucci, Levitt, Lund, et al. 2002; Stettler et al. 2002; Tanigawa et al. 2005).

Table 4
Basic measurements from OI response maps and labeling experiments

Measurement	Cat area 17	Monkey area V1
Active region density (mean ± standard deviation)	1.0 ± 0.2/mm^2	2.0 ± 0.2/mm^2
Number of active regions in OI map (mean ± standard deviation)	6.1 ± 3.2	59.2 ± 4.7
Number of patches in injection (mean ± standard deviation)	13.4 ± 2.1	13.1 ± 6.8
Interdomain distance (mode, 95% CI of mode)	1.01 [0.95–1.07] mm	0.74 [0.71–0.77] mm
Interdomain distance (mean ± standard deviation)	1.05 ± 0.25 mm	0.74 ± 0.18 mm
Interpatch distance (mode, 95% CI of mode)	0.90 [0.81–1.03] mm	0.50 [0.41–0.59] mm
Interpatch distance (mean ± stdandard deviation)	1.06 ± 0.39 mm	0.52 ± 0.17 mm
Interdomain neighbor angles (mode, 95% CI of mode)	57.8 [49.5–60.3] degree	60.6 [54.9–67.5] degree
Interpatch neighbor angles (mode, 95% CI of mode)	66.2 [58.5–83.7] degree	61.4 [54.9–65.7] degree

Note: See Tables 2 and 3 for details of the numbers of maps and injections obtained. We have reported modes for our measured distributions of interneighbor angles because the distributions themselves are highly skewed. CIs were estimated using a bootstrap analysis. See Figures 8 and 9 for plots of the full distributions. n = 13 injections and 266 response maps (cat area 17); 27 injections and 16 response maps (monkey V1).

A fundamental question is whether there is any consistent structure present in the arrangement of patches and active regions. We compared the distributions of angles measured over reconstructed patches against sets of points drawn from a Poisson model with the same density as that of patches (shown as dashed blue curves in Fig. 8; for details, see Materials and Methods). For both cat and monkey, the configuration of patch locations deviates significantly from their respective Poisson models ($P_{K\text{-}S} < 0.001$ in both cases). Evidence for distinct spatial structure is also present in the distributions of angles measured from OI response maps (see Fig. 9; $P_{K\text{-}S} < 0.001$ for cat and monkey). These results show very strongly that the arrangement of neither patches nor active regions is random.

Our measurements of shape indicate not merely nonrandomness in the arrangement of the anatomical and functional systems under analysis, but the strong overrepresentation of 60° angles formed both by patch spreads and by sets of active regions hints at an underlying hexagonal structure (see Figs 8 and 9). Reconstructions of the superficial patch system in primary visual cortex support this impression of a quasi-hexagonal arrangement (e.g., see Fig. 6*a*). We performed a more rigorous quantification of these putative lattice configurations by building models for random spatial arrangements of sets of points, with tunable amounts of regular structure. By varying a parameter δ, our models produce point configurations ranging from a perfect regular lattice to a Poisson distribution. We compared the measured patch and active region arrangements against random arrangements with hexagonal and square lattice structure. We used a value for jitter in our lattice models of δ = 0.5, corresponding to a maximum jitter distance for a single point of 50% of the nominal grid spacing. This value resulted in the best correspondence with our measured distributions. See Materials and Methods for more details of these models.

The result of comparisons between the spatial configuration of the patch system and both hexagonal and square lattices are shown in Figure 10*a–d*. The measured distributions are much more consistent with the hexagonal lattice model than the square lattice model ($P_{K\text{-}S} = 0.70$ vs. $P_{K\text{-}S} < 0.001$ in cat area 17; $P_{K\text{-}S} = 0.68$ vs. $P_{K\text{-}S} = 0.01$ in monkey V1). The same holds true for the spatial configuration of active regions (see Fig. 10*e,f*). In both species, the arrangement of active regions cannot be distinguished from the jittered hexagonal lattice model ($P_{K\text{-}S} = 0.10$ and $P_{K\text{-}S} = 0.28$ for cat and monkey, respectively) and differs significantly from the jittered square lattice model ($P_{K\text{-}S} < 0.01$ and $P_{K\text{-}S} < 0.001$ for cat and monkey, respectively). The superficial patch system shows a strong tendency toward a noisy hexagonal arrangement.

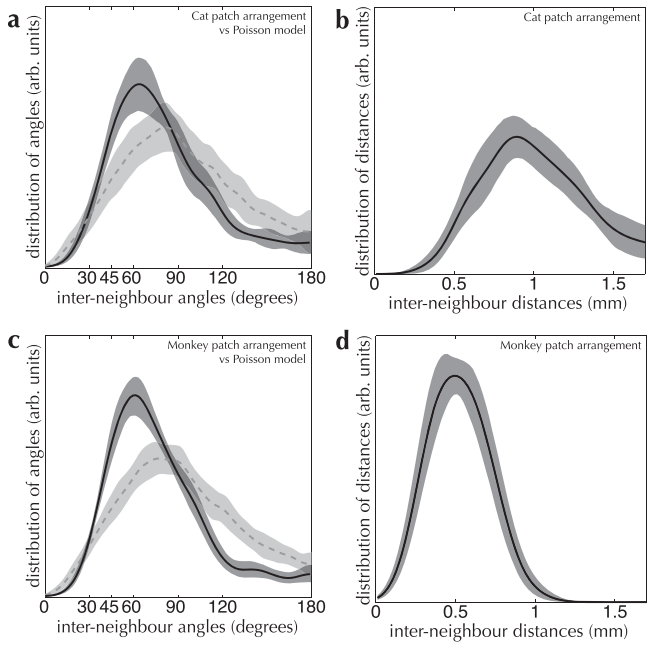

Figure 8. Distributions of interneighboring-patch angle and distance for cat (*a*,*b*) and monkey (*c*,*d*), measured over our database of patch-labeling injections. Distances between neighboring patches (shown in the right-hand graphs) and angles between sets of neighboring patches (left-hand graphs) were collected from reconstructions of patch-labeling injections, as described in Materials and Methods. The mean distribution is shown as a solid curve in all graphs; distribution variance (shaded regions) was estimated by computing the 90% bootstrap CI. For comparison, the angle distribution measured from a Poisson random model is shown by the dashed line for both Cat and Monkey. (*a* and *b*) Measurements over patch-labeling injections in Cat primary visual cortex (area 17). The measured distribution of interneighbor angles differs significantly from a Poisson distribution of the same intensity ($P_{K\text{-}S} < 0.001$). $n = 13$ injections. (*c* and *d*) Measurements over patch-labeling injections in Monkey area V1. The measured distribution of interneighbor angles differs significantly from a Poisson distribution of the same intensity ($P_{K\text{-}S} < 0.001$). $n = 27$ injections. 1000 bootstrap resampling runs were performed to estimate CIs for the distributions in all graphs.

Superficial Patch System Organization Compared with Functional Organization

Turning to the central point of this report, we examined the relationship between the superficial patch system and the

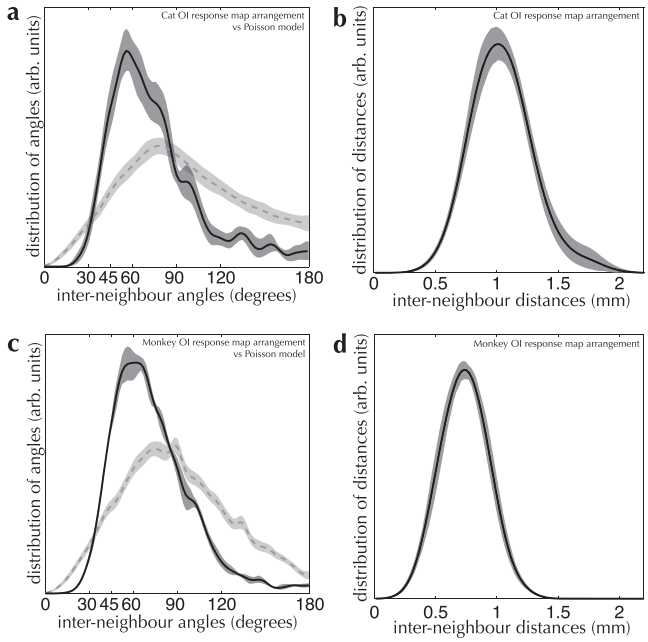

Figure 9. Spatial arrangement measurements for active regions on OI response maps for Cat (*a* and *b*) and Monkey (*c* and *d*). Conventions are the same as in Figure 8. (*a* and *b*) Measurements over Cat OI response maps. The measured distribution of interneighbor angles differs significantly from a Poisson distribution of the same intensity ($P_{K\text{-}S} < 0.001$). $n = 26$ imaging experiments, 266 maps total. (*c* and *d*) Measurements over Monkey OI response maps. The measured distribution of interneighbor angles differs significantly from a Poisson distribution of the same intensity ($P_{K\text{-}S} < 0.001$). $n = 4$ imaging experiments, 16 maps total. 1000 bootstrap resampling runs were performed to estimate CIs for the distributions in all graphs.

arrangement of function within primary visual cortex, in macaque monkey (shown in Fig. 11). The "shape" of patch spreads, as measured by the distribution of angles formed between neighboring patches, was the same as that measured for active regions ($P_{K\text{-}S}$ = 0.39). This indicates that the same spatial rule is followed in the arrangement of patches and functional domains across the surface of macaque monkey V1.

The only obvious difference we observed between labeled patches and the cortical response is in spacing of patches versus spacing of active regions, illustrated in Figure 11*b* and *c* (and see Table 4). In fact, we expect to observe a smaller average separation between patches than between active regions due to shrinkage of cortical tissue introduced either by fixation or by histological processing or both. Where linear shrinkage between live cortex and tissue slices processed for histology has been measured, values between 1% and 23% have been reported for cat cortical tissue (Beaulieu and Colonnier 1983; Lübke and Albus 1992a, 1992b; Kisvárday et al. 1994; Avendaño et al. 1995; Kisvárday et al. 1997) and between 10% and 45% for primate cortex (Robins et al. 1956; Hubel and Wiesel 1972; Rockland 1985a; Lund et al. 2003; Gilbert [personal communication]). Presumably, each injection into the superficial layers is a random sample from the same cortical patch system, regardless of the lab where it was performed. If our measured difference between patch and active region spacing was due to a true difference in spatial scale, then one would expect the distribution of interpatch spacings to be consistent between labs. In contrast, measurements from different labs show very different distributions (see Fig. 11*c*), providing evidence for a large variation in shrinkage between labs, presumably caused by differing processing techniques.

For most of the patch-labeling injections in our database, shrinkage was not measured or reported, so we could not correct for this in our analysis. However, studies where functional maps were aligned with patch injections by linear expansion show the same periodicities for labeled patches as for same orientation domains (Malach et al. 1993; Yoshioka et al. 1996; Stettler et al. 2002). For this reason, we believe that our measured difference in spacing, which reflects an average linear shrinkage of around 30% and falls within the reported range for tissue shrinkage, does not reflect a true difference between patch and active region spacing.

Cross-Species Comparison of Cortical Design

How similar is the "design" of cat and primate cortices? We examined this question from both an anatomical and a functional perspective by comparing our measurements of spatial arrangement across species (see Fig. 12). The conspicuous difference between cat and macaque monkey is one of scale: the density of patches and active regions doubles between cat and macaque visual cortex (see Table 4). Nevertheless, the arrangement of patches and active regions, as judged by our measurements of lattice shape, is strikingly conserved between species. The distributions of angles formed by patch spreads and by active regions follow the same distribution in cat and macaque monkey ($P_{K\text{-}S}$ = 0.20 for labeled patches, $P_{K\text{-}S}$ = 0.28 for active regions). This result indicates a strong similarity between cat and monkey in the mechanisms used to form representations in primary visual cortex.

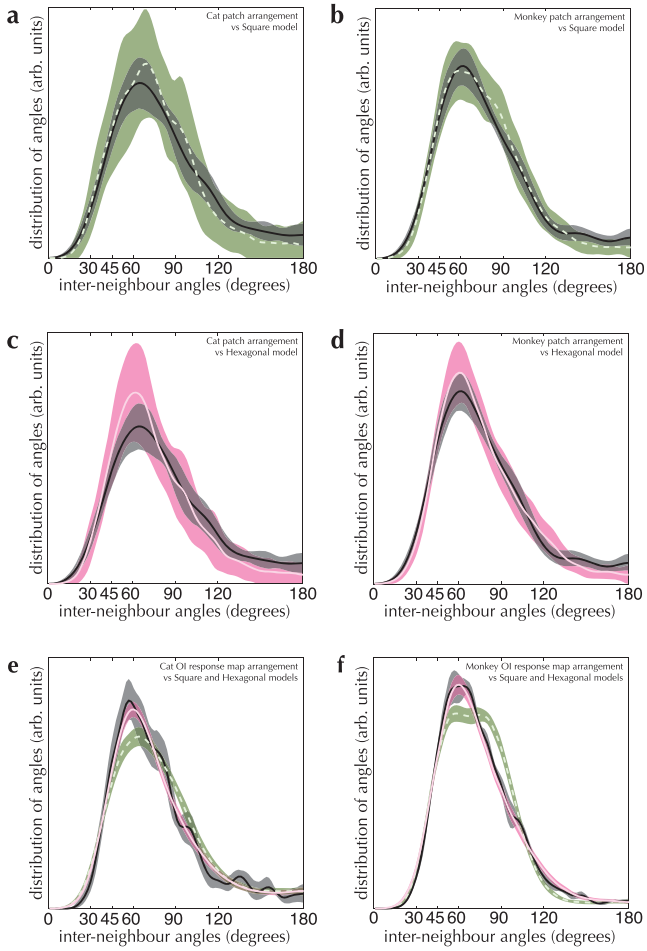

Figure 10. Comparison between angle distributions from OI response maps, patch-labeling experiments and lattice models. Distributions measured from the indicated experimental dataset are shown as solid black curves and dark shading in all graphs. (*a* and *b*) Interneighbor angle distributions measured from patch-labeling experiments (solid black curve and dark shading) compared with a square lattice model (dashed green curve and green shading). In cat area 17 (*a*), these distributions are significantly different ($P_{K\text{-}S} < 0.001$), while in monkey V1 (*b*), these distributions are marginally similar at a significance level of $\alpha = 1\%$ ($P_{K\text{-}S} = 0.01$). (*c* and *d*) Patch-labeling experiments (solid black curve and gray shading) compared with a hexagonal lattice model (solid magenta curve and shading). In cat area 17 (*c*), these distributions are indistinguishable ($P_{K\text{-}S} = 0.70$); the same is true in monkey V1 (*d*; $P_{K\text{-}S} = 0.68$). $n = 13$ injections in *a* and *c*, $n = 27$ injections in *b* and *d*. (*e* and *f*) Angle distributions measured from OI response maps (solid black curves and gray shading) compared with hexagonal (solid magenta curves and shading) and square (dashed green curves and green shading) lattice models. In both cat area 17 (*e*) and monkey V1 (*f*), the square lattice model differs significantly from the OI response map distributions ($P_{K\text{-}S} < 0.01$ for both cat and monkey primary visual cortex). In both cases, the hexagonal lattice model cannot be distinguished from the OI response map distributions ($P_{K\text{-}S} = 0.10$ for cat area 17, $P_{K\text{-}S} = 0.28$ for monkey V1). $n = 266$ response maps in *e*, $n = 16$ response maps in *f*. 1000 bootstrap resampling runs were performed to estimate the 90% CIs of each of the distributions (shaded regions in all graphs).

Discussion

We applied the statistical theory of shape to measurements of the spatial configuration of function and anatomy in neocortex. This allowed us to examine the superficial patch system and the arrangement of active regions in OI response maps for evidence of lattice structure, pooled across several experimental animals. Our measurements revealed a distinctive nonrandom arrangement in the way patches, and active regions spread across the surface of primary visual cortex—both

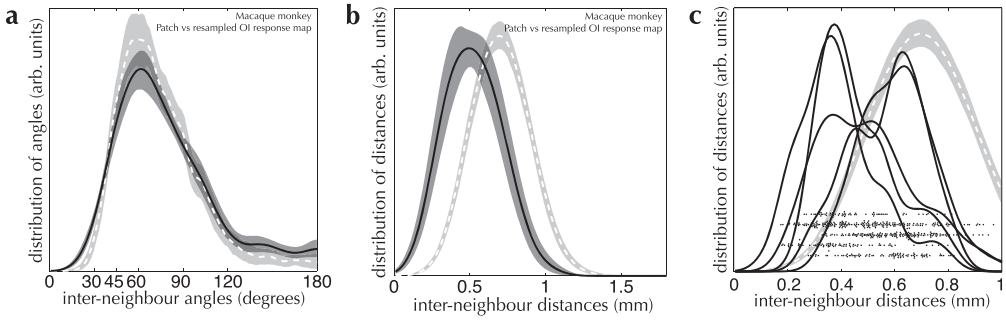

Figure 11. Comparison between the spatial arrangement of OI response maps and that of the superficial patch system in monkey V1. Sets of active regions from OI response maps from monkey V1 were resampled, using the convex hull of a group of patches as a mask (for details, see Materials and Methods). The spatial arrangement of these resampled response maps was then analyzed using the same characteristic measures as above. In all graphs, the distributions measured from our patch-labeling injection database are shown as solid curves with dark shading. The resampled OI response maps are represented by dashed curves and lighter shading. (*a*) The distributions of angles on the OI response maps are indistinguishable from that measured from the patch groups ($P_{K\text{-}S} = 0.39$; $n = 108$ resampled OI response maps, $n = 27$ injections). (*b*) The mean spacing measured between neighboring active regions on the OI response maps (dashed curves) is clearly different from that measured between neighboring patches (solid curve—0.74 mm vs. 0.50 mm, respectively). (*c*) The same data as shown in *b* but with the distributions of interpatch distance separated by lab (solid curves). The black points in *c* comprise a scatter plot for measured interpatch distances for each grouped set of injections, one row per source laboratory. These are included to illustrate the large variance in tissue shrinkage observed between different labs, assuming that all labs are sampling from the same patch system statistics. The dashed curve indicates the distribution of separations between active regions measured from resampled OI response maps, as in *b*, shown for comparison.

systems exhibited evidence for noisy hexagonal structure but not square lattice structure. More importantly, the configuration of labeled patches was strikingly similar to that of the cortical response to drifting grating stimuli. We also found that the design of area 17 is remarkably conserved between cat and macaque monkey, despite an almost 2-fold difference in density of patches and active regions between the 2 species.

Like-to-Like Connectivity within the Superficial Patch System

Many context-dependent and gestalt perceptual phenomena have been ascribed to the superficial patch system, driven by frequent observations of functional bias in the patch projections (for a review, see Gilbert 1992). In line with the dogma of like-connects-to-like, the majority of these phenomena require facilitatory interactions over large areas of visual space: for example, texture and curve continuity (Bosking et al. 1997; Schmidt et al. 1997; Ben-Shahar and Zucker 2004), color constancy (Gilbert 1992), illusory contours (Gilbert 1992), and feature binding and scene segmentation through promotion of synchronized oscillatory activity (Gray et al. 1989; Engel et al. 1990; Gray, Engel, et al. 1990; Gray, König, et al. 1990). Unfortunately, the necessity of the superficial patch system has not been demonstrated for any of these feats of visual processing.

Like-connects-to-like connectivity was originally proposed for the superficial patch system by Mitchison and Crick (1982), as a mechanism for generating complex receptive fields in layers 2 and 3 of primary visual cortex. Their hypothesis proved remarkably prescient: a bias toward connecting areas of similar function was subsequently demonstrated for orientation preference in area 17 (Malach et al. 1993; Bosking et al. 1997; Schmidt et al. 1997; Stettler et al. 2002), for the cytochrome oxidase (CO)–rich blobs in the superficial layers of area 17 (Rockland and Lund 1983; Livingstone and Hubel 1984b; Burkhalter and Bernardo 1989; Malach et al. 1993; Yoshioka et al. 1996), and for other functional modalities in a range of sensory and motor areas.

However, the beguiling simplicity of the "like-to-like" concept appears less than satisfactory when one examines the numbers

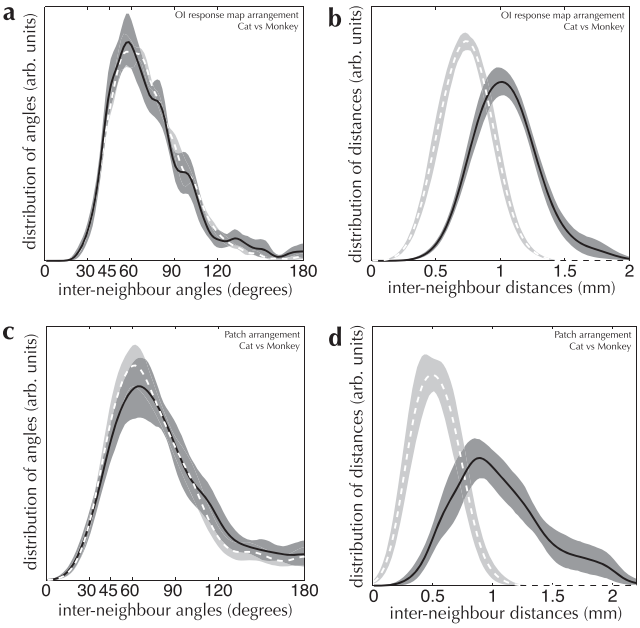

Figure 12. Cross-species comparison of the spatial structure of OI response maps and patch spreads (*a* and *b*) Measured interneighbor angle (*a*) and distance (*b*) distributions from OI response maps in cat area 17 (dashed curve and light shading) and monkey V1 (solid curve and dark shading). Despite a large difference in spatial scale between cat and monkey (mode interneighbor distances of 1.01 mm and 0.74 mm, respectively), the spatial arrangement of active domains is indistinguishable ($P_{K\text{-}S} = 0.28$; $n = 266$ maps in cat area 17, 16 maps in monkey V1). (*c* and *d*) Interneighbor angle (*c*) and distance (*d*) distributions from patch-labeling injections in cat area 17 (light dashed curves) and monkey V1 (dark solid curves). Once again, the difference in spatial scale is marked (0.90 mm vs. 0.50 mm for cat and monkey, respectively), while the spatial arrangement of patch locations is indistinguishable ($P_{K\text{-}S} = 0.20$; $n = 13$ injections in cat area 17, 27 injections in monkey V1).

in detail. Between 35% and 40% of clustered labeling falls in regions responsive to orientations outside those preferred by neurons at the injection site; that is, a weak functional bias that implies the anatomical location of patch projections is considerably less tuned than the physiological orientation preference of the cells making those projections (Malach et al. 1993;

Bosking et al. 1997; Stettler et al. 2002). Measurements over other modalities in visual cortex show similar divergence in the functional bias of patch projections, leading to the conclusion that like often does not connect to like.

In fact, the restrictive connectivity implied by a strong interpretation of the term like-to-like does not exist in the superficial patch system. Connected regions in primary visual cortex are only "like" when examined from the point of view of particular functional properties. When receptive field position is also considered, the projections that form the patch system are certainly not between regions of like response, as has been frequently noted (Rockland et al. 1982; Allman et al. 1985; Gilbert 1992; Angelucci, Levitt, Walton, et al. 2002; Stettler et al. 2002 and many other studies; see the papers referenced above). The alternative hypothesis we present here is that regions encompassing a set of labeled patches are connected simply because they are often coactivated (a Hebbian-like point of view). That the activity of several discrete regions of visual cortex spanning several millimeters might be correlated is implied by the statistical structure of the visual world, regardless of intracortical connectivity. Since a visual stimulus is often composed of noninfinitesimal regions of constant functional properties, nearby regions of cortex that have receptive fields at different locations but with similar functional properties will be coactivated. Indeed, correlated firing occurs at discrete points in visual cortex with similar but non-overlapping receptive fields due to common input (Ts'o et al. 1986). We propose that cortical activation patterns that occur frequently are connected by the clustered projections of the patch system. Our hypothesis does not imply an experience-driven developmental mechanism but does require patterned spatial activity in cortex during the formation of the patch system (Grabska-Barwińska and von der Malsburg 2008).

The general relationship we propose between the superficial patch system and the spatial arrangement of cortical function is compatible with but not identical to that implied by the like-to-like hypothesis. For example, in Inferotemporal (IT) cortex, connections between objects and forms that often occur together but are not like (such as regions encoding for heads and regions encoding for bodies) would be clearly beneficial for promoting the recognition of compound objects (Wang et al. 1996; Tsunoda et al. 2001). We predict that regions of IT cortex coactivated by a complex, but familiar, object will fall over a set of anatomically connected patches, but activated regions may cover only a subset of the patches labeled from an injection into any one active region. A corollary of our hypothesis is that all regions of cortex that have a patch system should also show modular activation.

Self-Consistent Cortical States and the Patch System

Oriented grating stimuli provide an input that requires encoding of identical stimulus parameters over the extent of the visual field—we call this a self-consistent stimulus, since the stimulus parameters at any point are consistent with those across the entire visual field. The cortical response to these stimuli requires the encoding of identical values for functional parameters over the surface of visual cortex. We call the evoked states self-consistent cortical states, since any active region in primary visual cortex encodes values for functional parameters that are consistent with any other concurrently active region in primary visual cortex.

We have shown here that the cortical state corresponding to a self-consistent stimulus has the same spatial organization as the superficial patch system. We conclude that the superficial patch system is the physical substrate for promoting self-consistent cortical states. Patch connections will bias the cortical state toward coactivation of regions encoding for mutually consistent functional representations. This point allows a functional interpretation to be placed on the patterns of labeling seen following injections of tracers into cortex. The patch system provides a physical encoding for statistical properties of the modality represented in an area of cortex. A set of concurrently labeled patches participate in a network composed of mutually consistent representations of cortical input. Regions of cortex that form a set of concurrently labeled patches will not always be activated simultaneously but are more likely to be simultaneously active than unconnected regions.

This interpretation of the patch system as promoting concurrent activity of colabeled patch locations follows from related work, exploring the effect of patterned lateral excitatory projection lattices on activity states in a simulated cortical network. A projection system with properties similar to the superficial patch system promotes concurrent spontaneous activation of connected regions, in a simulated cortical network with realistic lateral connectivity and biophysical time constants (Muir and Douglas, in preparation). Population activity in cortex is thereby biased toward states that reflect the spatial configuration of the underlying lattice. Previous work by one of the authors of the present study showed that spontaneously emerging cortical states indeed have the same spatial arrangement as orientation-selective responses in the same animal (Kenet et al. 2003). The present work strongly indicates that the spontaneously emerging cortical states observed by Kenet and colleagues have the same spatial arrangement as the superficial patch system and strengthens the argument for a direct determination of domain configuration by the patch system.

Previous Characterizations of the Cortical Response

A handful of previous studies have examined the shape of the functional response in primary visual cortex, over and above a simple analysis of periodicity. McLoughlin and Schiessl (2006) performed an autocorrelation analysis of the orientation-selective response to examine periodicity in marmoset primary and secondary visual cortex. Their results show some evidence for a roughly hexagonal arrangement of domains, which they unfortunately leave unremarked. Obermayer and Blasdel (1993, 1997) examined orientation pinwheel locations in macaque monkey visual cortex, comparing Fourier spectra of orientation pinwheel locations with spectra produced by regular hexagonal and square lattices. They did not observe evidence for regular lattice structure in the arrangement of either orientation preference domains or pinwheel locations. Ohki et al. (2000) performed a similar analysis, exploring the arrangement of orientation pinwheels close to the area 17/18 border in cat visual cortex and also found no evidence for a global regular lattice structure in the spatial arrangement of pinwheels. Although we did not examine the arrangement of pinwheels, one might assume that pinwheels and iso-orientation domains would have related spatial configurations, and so at face value our results and those presented above appear to differ. However, these researchers did not compare their measured arrangements with noisy, nonregular lattice patterns as we have done and do not show that their analysis

is sensitive to patterns that show only quasi-regular spatial structure. We have shown that the true arrangement of orientation domains is indeed not perfectly regular but is nevertheless far from random.

Spatial analyses of the type performed by these researchers will identify the presence of global lattice structure, while neglecting local structure present between adjacent points of interest. Our analysis is sensitive to local lattice structure and to the precise form of deviation from global structure, both of which we have shown to be important in characterizing the arrangement of anatomical and functional units in cortex.

Modular Responses across Cortex

Quasiperiodic activation patterns in response to a stimulus are not restricted to primary visual cortex. In cats, old- and new-world monkeys, ferrets and probably many other mammalian species, primary sensory and motor areas all reveal a modular arrangement of function overlaid on a topographic map, with the possible exception of the less-understood areas devoted to audition (Versnel et al. 2002; Ojima et al. 2005; but see Nelken et al. 2004, 2008). This patterned arrangement is particularly clear in primary visual cortex, where repeated modules respond preferentially to different aspects of a visual stimulus. The periodicity of these regions of activity is not related to periodic features of a stimulus but appears to be characteristic for a region of cortex. This is intuitively obvious for somatosensory cortex, for which a single point on the skin surface can be stimulated. Doubts could be raised, however, for the oriented grating stimuli we have used, which intrinsically contain periodic spatial energy. Nevertheless, gratings produce patterns with the same rough periodicity over a wide range of spatial frequencies (Blasdel 1992; Bonhoeffer et al. 1995; Hübener et al. 1997; Issa et al. 2000). Oriented bars provoke a cortical response that is periodic along the cortical projection axis of the bar (Bosking et al. 2002), contrary to the effect that would be predicted if the periodic spatial energy in a stimulus drove cortex to adopt a periodic response. Other nongrating stimuli, such as uniform surfaces (Tani et al. 2003), iso-luminant and colured stimuli (Landisman and Ts'o 2002; Lu and Roe 2008), and illusory contours (Sheth et al. 1996; Ramsden et al. 2001) also elicit punctate responses from primary visual cortex. Our results therefore apply generally to primary visual cortex and not just to the particular parameters of our stimuli.

Punctate cortical responses are by no means restricted to primary sensory areas of neocortex. The various CO compartments in area 18 divide the cortical surface in a modular arrangement of preference for different qualities of a visual stimulus (disparity—Chen et al. 2008; changes in luminance—Lu and Roe 2007; Wang et al. 2007; and color—Wang et al. 2007; Lu and Roe 2008). Modular maps are present further up the visual hierarchy (cat area 21—Huang et al. 2006; primate area V4—Ghose and Ts'o 1997; and MT—Malonek et al. 1994; Malach et al. 1997; Xu et al. 2004, 2006). In vivo intracortical microstimulation reveals punctate arrangements of function and of electrically driven responses in macaque monkey motor (Huntley and Jones 1991), premotor (Sawaguchi 1994), and prefrontal cortex (Sawaguchi 1996). If the relationship between the superficial patch system and the function holds as a general cortical feature, then we expect the same correspondence of spatial configuration will be observed in these other areas of cortex.

IT cortex contains a particularly interesting example of a modular functional architecture. Regions across area IT respond to particular objects placed in the visual field, with a large degree of invariance to position and size (Tanaka 2003). Progressively increasing the complexity of an object, or adding more parts to build a compound object, recruits more punctate modules to the cortical representation (Wang et al. 1996; Tsunoda et al. 2001). The arrangement of these modules is less periodic than for orientation domains in primary visual cortex, and the appearance of patch-labeling injections in area IT qualitatively echoes this less regular spatial arrangement of function (Fujita and Fujita 1996; Fujita 2002; Tanigawa et al. 2005), but a concerted data collection effort is required before a quantitative analysis of the form presented here will be possible.

Analysis Sensitivity

We observed no difference between the respective spatial arrangements of the superficial patch system and of function in macaque monkey primary visual cortex, as well as no difference between the layout of cat and monkey primary visual cortices. These findings rely on the ability of our analysis to extract statistical shape and on the sensitivity of the K–S test to compare these statistical measures. Our choice of a Gabriel graph to define neighbor relations introduces a bias against small interneighbor angles, when compared against measurements made over a Delaunay triangulation; very acute angles correspond to long, thin Delaunay triangles, which are usually excluded from Gabriel graphs due to the neighbor criterion used. We performed the same comparisons as illustrated in this report using a neighbor relation based on a Delaunay triangulation. Comparing spatial arrangements of patches and domains measured using Delaunay neighbor graphs gave qualitatively similar results to measurements using Gabriel graphs, but the Delaunay neighbor relation was more susceptible to border artifacts.

We observed empirically that the K–S test was extremely sensitive to differences in the distributions of angles that we used to characterize spatial arrangements. For example, we were easily able to differentiate between artificial sets of points with underlying hexagonal and square lattice structure, even with large amounts of jitter. This is a difficult task for a human observer (see Fig. 4). In practice, when comparing even slightly differing distributions—such as 2 hexagonal grids with jitter of $\delta = 0.4$ and $\delta = 0.5$—the asymptotic P value estimates for the K–S test dropped to values extremely close to zero ($P \approx 10^{-40}$, $n = 100$ simulated OI maps). It is therefore not the case that any roughly periodic arrangement will look similar under our analysis. The smaller number of maps we recorded from macaque V1 did not cause a problem for our measurements, as the higher density and larger areas imaged in the monkey produced many more observable active regions per map than present in the maps from cat area 17 (see Table 4).

It is theoretically possible that the patch system and functional arrangement could have identical distributions under our analysis but still show no physical relationship between patch and active region locations in the same animal. This could occur, for example, if every patch was offset in

space by a common displacement from a corresponding active region. Such an arrangement seems unlikely, and the demonstration of a weak bias toward like-to-like patch projections in single animals by other researchers indicates that at least some degree of correspondence between patches and functional domains exists (Malach et al. 1993; Bosking et al. 1997; Schmidt et al. 1997; Stettler et al. 2002).

In our analysis, we assumed that each blank-subtracted single-condition response map was independent. This assumption would be unfounded if the average representation of oriented stimuli were inhomogeneous in primary visual cortex. For example, if some points in visual cortex responded strongly to stimuli of any orientation, these same locations would be present in each single-condition map and would distort our statistical measurements of the cortical response. We examined this issue in cat area 17 and found that our assumption of a homogenous representation of orientation was justified (see Supplementary Methods).

Evolution of Cortical Structure

We have shown that cats and macaque monkeys share at least 2 features of primary visual cortex, down to the spatial arrangement of functional and anatomical units. Since the feline (Laurasiatherian) and primate (Euarchontoglires—Supraprimate) ancestor lines diverged 90–107 million years ago (Murphy et al. 2001; Springer et al. 2003), this implies that either the required developmental machinery was already in place in the common ancestor or that cortical maps with remarkably similar structure emerged through convergent evolution in these 2 lines. Other features of functional maps in area 17, similarly relying on long-range cortical interactions, are conserved between the ferret (Carnivora; the same order as cats), tree shrew (grand order Euarchonta; closely related to primates), and galago (order Primate) (Kaschube et al. 2010).

The common design of visual cortex between species that are only distantly related raises an interesting question for rodents, which are more closely related to primates than primates are to cats (Springer et al. 2003). Despite their closer genetic relationship to primates, rodents do not have smooth maps of orientation preference or a superficial patch system as presented here (Van Hooser et al. 2006). Has the design of rodent cortex degenerated to the extent that it has lost the ability to form these systems? Alternatively, the required mechanisms may still be present but express themselves differently due to a change in one or more developmental parameters—for example, the smaller size of visual cortex or the degree of like-to-like preference exhibited by superficial layer neurons (Koulakov and Chklovskii 2001).

We have presented a new set of evidence for the relationship between the superficial patch system and cortical function. We showed that both the patch system and the cortical response display a well-defined signature of their spatial configurations, and that this spatial configuration is shared between the anatomical and the functional systems. The projections that comprise the superficial patch system define the spatial layout of coactive domains across the cortical surface. This fact suggests a new interpretation for the patch system—that the clustered projections provide a physical encoding for statistical properties of the cortical response. Concurrently labeled patches in area 17 promote the expression of cortical activity states that correspond to statistical expectations of regularity in the visual world. The superficial patch system is a mechanism for ensuring consistency between the cortical response to potentially ambiguous stimuli and an internal model of the world.

Supplementary Material

Supplementary material can be found at:http://www.cercor.oxfordjournals.org/

Funding

European Commission (FP6 2005-015803 DAISY to D.R.M., E.R., Kevan Martin, A.G., and R.J.D.) and John Crampton Travelling Scholarship to D.R.M.

Notes

The authors wish to thank Kevan Martin, Daniel Kiper, and Melissa Penny for their feedback and critiques, and members of the Institute for Neuroinformatics for helpful discussions. The analysis was designed by D.R.M. and R.J.D. and performed by D.R.M. Experiments were performed by N.M.A.Da.C., C.G., and E.R. in the lab of Kevan Martin and by S.M. and D.B.O. in the lab of A.G. The manuscript was written by D.R.M. *Conflict of Interest*: None declared.

References

Albus K, Sieber B. 1984. On the spatial arrangement of iso-orientation bands in the cat's visual cortical areas 17 and 18: a 14C-deoxyglucose study. Exp Brain Res. 56:384–388.

Allman J, Miezin F, McGuinness E. 1985. Direction- and velocity-specific responses from beyond the classical receptive field in the middle temporal visual area (MT). Perception. 14:105–126.

Amir Y, Harel M, Malach R. 1993. Cortical hierarchy reflected in the organization of intrinsic connections in macaque monkey visual cortex. J Comp Neurol. 334:19–46.

Angelucci A, Levitt JB, Lund JS. 2002. Anatomical origins of the classical receptive field and modulatory surround field of single neurons in macaque visual cortical area V1. Prog Brain Res. 136: 373–388.

Angelucci A, Levitt JB, Walton EJS, Hupé J-M, Bullier J, Lund JS. 2002. Circuits for local and global signal integration in primary visual cortex. J Neurosci. 22:8633–8646.

Angelucci A, Sainsbury K. 2006. Contribution of feedforward thalamic afferents and corticogeniculate feedback to the spatial summation area of macaque V1 and LGN. J Comp Neurol. 498:330–351.

Asi H, Levitt JB, Lund JS. 1996. In macaque V1 lateral connections in layer 4B have a different topography than in layers 2/3. Soc Neurosci Abstr. 26:1608.

Avendaño C, Roda JM, Carceller F, Díez-Tejedor E. 1995. Morphometric study of focal cerebral ischemia in rats: a stereological evaluation. Brain Res. 673:83–92.

Beaulieu C, Colonnier M. 1983. The number of neurons in the different laminae of the binocular and monocular regions of area 17 of the cat. J Comp Neurol. 217:337–344.

Ben-Shahar O, Zucker S. 2004. Geometrical computations explain projection patterns of long-range horizontal connections in visual cortex. Neural Comput. 16:445–476.

Blasdel GG. 1992. Differential imaging of ocular dominance and orientation selectivity in monkey striate cortex. J Neurosci. 12: 3115–3138.

Bonhoeffer T, Grinvald A. 1991. Iso-orientation domains in cat visual cortex are arranged in pinwheel-like patterns. Nature. 353:429–431.

Bonhoeffer T, Kim D-S, Malonek D, Shoham D, Grinvald A. 1995. Optical imaging of the layout of functional domains in area 17 and across the area 17/18 border in cat visual cortex. Eur J Neurosci. 7:1973–1988.

Boots BN. 1974. Delaunay triangles: an alternative approach to point pattern analysis. Proc Assoc Am Geogr. 6:26–29.

Bosking WH, Crowley JC, Fitzpatrick D. 2002. Spatial coding of position and orientation in primary visual cortex. Nat Neurosci. 5:874–882.
Bosking WH, Zhang Y, Schofield B, Fitzpatrick D. 1997. Orientation selectivity and the arrangement of horizontal connections in tree shrew striate cortex. J Neurosci. 17:2112–2127.
Boyd J, Matsubara JA. 1991. Intrinsic connections in cat visual cortex: a combined anterograde and retrograde tracing study. Brain Res. 560:207–215.
Burkhalter A, Bernardo KL. 1989. Organization of corticocortical connections in human visual cortex. Proc Natl Acad Sci U S A. 86:1071–1075.
Callaway EM, Katz LC. 1990. Emergence and refinement of clustered horizontal connections in cat striate cortex. J Neurosci. 10: 1134–1153.
Chen G, Lu HD, Roe AW. 2008. A map for horizontal disparity in monkey V2. Neuron. 58:442–450.
Coogan TA, Van Essen DC. 1996. Development of connections within and between areas V1 and V2 of macaque monkeys. J Comp Neurol. 372:327–342.
Cusick CG, Kaas JH. 1988a. Cortical connections of area 18 and dorsolateral visual cortex in squirrel monkeys. Vis Neurosci. 1:211–237.
Cusick CG, Kaas JH. 1988b. Surface view patterns of intrinsic and extrinsic cortical connections of area 17 in a prosimian primate. Brain Res. 458:383.
Diao Y-C, Jia W-G, Swindale NV, Cynader MS. 1990. Functional organization of the cortical 17/18 border region in the cat. Exp Brain Res. 79:271–282.
Douglas RJ, Martin KAC. 2004. Neuronal circuits of the neocortex. Annu Rev Neurosci. 27:419–451.
Efron B. 1979. Bootstrap methods: another look at the jackknife. The 1977 Rietz lecture. Ann Stat. 7:1–26.
Engel AK, König P, Gray CM, Singer W. 1990. Stimulus-dependent neuronal oscillations in cat visual cortex: inter-columnar interaction as determined by cross-correlation analysis. Eur J Neurosci. 2:588–606.
Fisken RA, Garey LJ, Powell TPS. 1975. The intrinsic, association and commissural connections of area 17 of the visual cortex. Philos Trans R Soc Lond B Biol Sci. 272:487–536.
Fujita I. 2002. The inferior temporal cortex: architecture, computation and representation. J Neurocytol. 31:359–371.
Fujita I, Fujita T. 1996. Intrinsic connections in the macaque monkey inferior temporal cortex. J Comp Neurol. 368:467–486.
Gabriel KR, Sokal RR. 1969. A new statistical approach to geographic variation analysis. Syst Zool. 18:259–278.
Galuske RAW, Schlote W, Bratzke H, Singer W. 2000. Interhemispheric asymmetries of the modular structure in human temporal cortex. Science. 289:1946–1949.
Ghose GM, Ts'o DY. 1997. Form processing modules in primate area V4. J Neurophysiol. 77:2191–2196.
Gilbert CD. 1992. Horizontal integration and cortical dynamics. Neuron. 9:1–13.
Gilbert CD, Wiesel TN. 1983. Clustered intrinsic connections in cat visual cortex. J Neurosci. 3:1116–1133.
Gilbert CD, Wiesel TN. 1989. Columnar specificity of intrinsic horizontal and corticocortical connections in cat visual cortex. J Neurosci. 9:2432–2442.
Grabska-Barwińska A, von der Malsburg C. 2008. Establishment of a scaffold for orientation maps in primary visual cortex of higher mammals. J Neurosci. 28:249–257.
Gray CM, Engel AK, König P, Singer W. 1990. Stimulus-dependent neuronal oscillations in cat visual cortex: receptive field properties and feature dependence. Eur J Neurosci. 2:607–619.
Gray CM, König P, Engel AK, Singer W. 1989. Oscillatory responses in cat visual cortex exhibit inter-columnar synchronization which reflects global stimulus properties. Nature. 338:334–337.
Gray CM, König P, Engel AK, Singer W. 1990. Synchronization of oscillatory responses in visual cortex: a plausible mechanism for scene segmentation. In: Haken H, Stadler M, editors. Synergetics of cognition. Berlin (Germany): Springer-Verlag. p. 82–98.
Grinvald A, Frostig RD, Siegel RM, Bartfeld E. 1991. High-resolution optical imaging of functional brain architecture in the awake monkey. Proc Natl Acad Sci U S A. 88:11559–11563.
Grinvald A, Lieke E, Frostig RD, Gilbert CD, Wiesel TN. 1986. Functional architecture of cortex revealed by optical imaging of intrinsic signals. Nature. 324:361–364.
Huang L, Shou T, Chen X, Yu H, Sun C, Liang Z. 2006. Slab-like functional architecture of higher order cortical area 21a showing oblique effect of orientation preference in the cat. Neuroimage. 32:1365–1374.
Hubel DH, Wiesel TN. 1972. Laminar and columnar distribution of geniculo-cortical fibers in the macaque monkey. J Comp Neurol. 146:421–450.
Hübener M, Shoham D, Grinvald A, Bonhoeffer T. 1997. Spatial relationships among three columnar systems in cat area 17. J Neurosci. 17:9270–9284.
Huntley GW, Jones EG. 1991. Relationship of intrinsic connections to forelimb movement representations in monkey motor cortex: a correlative anatomic and physiological study. J Neurophysiol. 66:390–413.
Issa NP, Trepel C, Stryker MP. 2000. Spatial frequency maps in cat visual cortex. J Neurosci. 20:8504–8514.
Jones EG, Wise SP. 1977. Size, laminar and columnar distribution of efferent cells in the sensory-motor cortex of monkeys. J Comp Neurol. 175:391–438.
Juliano SL, Whitsel BL, Tommerdahl M, Cheema SS. 1989. Determinants of patchy metabolic labeling in the somatosensory cortex of cats: a possible role for intrinsic inhibitory circuitry. J Neurosci. 9:1–12.
Kaas JH, Krubitzer LA, Johanson KL. 1989. Cortical connections of areas 17 (V-I) and 18 (V-II) of squirrels. J Comp Neurol. 281:426–446.
Karube F, Kisvárday ZF. 2010. Axon topography of layer IV spiny cells to orientation map in the cat primary visual cortex (area 18). Cereb Cortex. Advance Access published November 9, doi:10.1093/cercor/bhq232.
Kaschube M, Schnabel M, Löwel S, Coppola DM, White LE, Wolf F. 2010. Universality in the evolution of orientation columns in the visual cortex. Science. 330:1113–1116.
Kenet T, Bibitchkov D, Tsodyks M, Grinvald A, Arieli A. 2003. Spontaneously emerging cortical representations of visual attributes. Nature. 425:954–956.
Kisvárday ZF, Eysel UT. 1992. Cellular organization of reciprocal patchy networks in layer III of cat visual cortex (area 17). Neuroscience. 46:275–286.
Kisvárday ZF, Kim D-S, Eysel UT, Bonhoeffer T. 1994. Relationship between lateral inhibitory connections and the topography of the orientation map in cat visual cortex. Eur J Neurosci. 6:1619–1632.
Kisvárday ZF, Tóth É, Rausch M, Eysel UT. 1997. Orientation-specific relationship between populations of excitatory and inhibitory lateral connections in the visual cortex of the cat. Cereb Cortex. 7:605–618.
Kolmogorov A. 1933. Sulla determinazione empirica di una legge di distributione. G Ist Ital Attuari. 4:1–11.
Koulakov AA, Chklovskii DB. 2001. Orientation preference patterns in mammalian visual cortex: a wire length minimization approach. Neuron. 29:519–527.
Kritzer MF, Goldman-Rakic PS. 1995. Intrinsic circuit organization of the major layers and sublayers of the dorsolateral prefrontal cortex in the rhesus monkey. J Comp Neurol. 359:131–143.
Landisman CE, Ts'o DY. 2002. Color processing in macaque striate cortex: relationships to ocular dominance, cytochrome oxidase, and orientation. J Neurophysiol. 87:3126–3137.
Levitt JB, Yoshioka T, Lund JS. 1994. Intrinsic cortical connections in macaque visual area V2: evidence for interaction between different functional streams. J Comp Neurol. 342:551–570.
Lewis DA, Melchitzky DS, Burgos G-G. 2002. Specificity in the functional architecture of primate prefrontal cortex. J Neurocytol. 31:265–276.
Lewis JP. 1995. Fast normalized cross-correlation. Proc. of Vision Interface. 95:120–123.
Livingstone MS, Hubel DH. 1984a. Anatomy and physiology of a color system in the primate visual cortex. J Neurosci. 4:309–356.
Livingstone MS, Hubel DH. 1984b. Specificity of intrinsic connections in primate primary visual cortex. J Neurosci. 4:2830–2835.
Löwel S, Singer W. 1992. Selection of intrinsic horizontal connections in the visual cortex by correlated neuronal activity. Science. 255:209–212.

Lu HD, Roe AW. 2007. Optical imaging of contrast response in macaque monkey V1 and V2. Cereb Cortex. 17:2675–2695.
Lu HD, Roe AW. 2008. Functional organization of color domains in V1 and V2 of macaque monkey revealed by optical imaging. Cereb Cortex. 18:516–533.
Lübke J, Albus K. 1992a. Lack of exuberance in clustered intrinsic connections in the striate cortex of one-month-old kitten. Eur J Neurosci. 4:189–192.
Lübke J, Albus K. 1992b. Rapid rearrangement of intrinsic tangential connections in the striate cortex of normal and dark-reared kittens: lack of exuberance beyond the second postnatal week. J Comp Neurol. 323:42–58.
Luhmann HJ, Millán LM, Singer W. 1986. Development of horizontal intrinsic connections in cat striate cortex. Exp Brain Res. 63:443–448.
Luhmann HJ, Singer W, Martinez-Millán L. 1990. Horizontal interactions in cat striate cortex: I. Anatomical substrate and postnatal development. Eur J Neurosci. 2:344–357.
Lund JS, Angelucci A, Bressloff PC. 2003. Anatomical substrates for functional columns in macaque monkey primary visual cortex. Cereb Cortex. 13:15–24.
Lund JS, Yoshioka T, Levitt JB. 1993. Comparison of intrinsic connectivity in different areas of macaque monkey cerebral cortex. Cereb Cortex. 3:148–162.
Malach R, Amir Y, Harel M, Grinvald A. 1993. Relationship between intrinsic connections and functional architecture revealed by optical imaging and in vivo targeted biocytin injections in primate striate cortex. Proc Natl Acad Sci U S A. 90: 10469–10473.
Malach R, Schirman TD, Harel M, Tootell RBH, Malonek D. 1997. Organization of intrinsic connections in owl monkey area MT. Cereb Cortex. 7:386–393.
Malach R, Tootell RBH, Malonek D. 1994. Relationship between orientation domains, cytochrome oxidase stripes, and intrinsic horizontal connections in squirrel monkey area V2. Cereb Cortex. 4:151–165.
Malonek D, Tootell RBH, Grinvald A. 1994. Optical imaging reveals the functional architecture of neurons processing shape and motion in owl monkey area MT. Proc R Soc Lond B Biol Sci. 258:109–119.
Massey FJJ. 1951. The Kolmogorov–Smirnov test for goodness of fit. J Am Stat Assoc. 46:68–78.
Matsubara JA, Cynader MS, Swindale NV. 1987. Anatomical properties and physiological correlates of the intrinsic connections in cat area 18. J Neurosci. 7:1428–1446.
Matsubara JA, Cynader MS, Swindale NV, Stryker MP. 1985. Intrinsic projections within visual cortex: evidence for orientation-specific local connections. Proc Natl Acad Sci U S A. 82:935–939.
Matsubara JA, Phillips DP. 1988. Intracortical connections and their physiological correlates in the primary auditory cortex (AI) of the cat. J Comp Neurol. 268:38–48.
McGuire BA, Gilbert CD, Rivlin PK, Wiesel TN. 1991. Targets of horizontal connections in macaque primary visual cortex. J Comp Neurol. 305:370–392.
McLoughlin N, Schiessl I. 2006. Orientation selectivity in the common marmoset (Callithrix jacchus): the periodicity of orientation columns in V1 and V2. Neuroimage. 31:76–85.
Mitchison G, Crick F. 1982. Long axons within the striate cortex: distribution, orientation and patterns of connections. Proc Natl Acad Sci U S A. 79:3661–3665.
Muir DR, Douglas R. 2010. From neural arbors to daisies. Cereb Cortex. Advance Access published September 30, doi:10.1093/cercor/bhq184.
Murphy WJ, Eizirik E, O'Brien SJ, Madsen O, Scally M, Douady CJ, Teeling E, Ryder OA, Stanhope MJ, de Jong WW, et al. 2001. Resolution of the early placental mammal radiation using Bayesian phylogenetics. Science. 294:2348–2351.
Nelken I, Bizley JK, Nodal FR, Ahmed B, King AJ, Schnupp JW. 2008. Responses of auditory cortex to complex stimuli: functional organization revealed using intrinsic optical signals. J Neurophysiol. 99:1928–1941.
Nelken I, Bizley JK, Nodal FR, Ahmed B, Schnupp JW, King AJ. 2004. Large-scale organization of ferret auditory cortex revealed using continuous acquisition of intrinsic optical signals. J Neurophysiol. 92:2574–2588.
Neyman J, Scott EL. 1958. Statistical approach to problems of cosmology. J R Stat Soc B. 21:1–43.
Obermayer K, Blasdel GG. 1993. Geometry of orientation and ocular dominance columns in monkey striate cortex. J Neurosci. 13:4114–4129.
Obermayer K, Blasdel GG. 1997. Singularities in primate orientation maps. Neural Comput. 9:555–575.
Ohki K, Matsuda Y, Ajima A, Kim D-S, Tanaka S. 2000. Arrangement of orientation pinwheel centers around area 17/8 transition zone in cat visual cortex. Cereb Cortex. 10:593–601.
Ojima H, Takayanagi M. 2004. Cortical convergence from different frequency domains in the cat primary auditory cortex. Neuroscience. 126:203–212.
Ojima H, Takayanagi M, Potapov D, Homma R. 2005. Isofrequency band-like zones of activation revealed by optical imaging of intrinsic signals in the cat primary auditory cortex. Cereb Cortex. 15: 1497–1509.
Puckak ML, Levitt JB, Lund JS, Lewis DA. 1996. Patterns of intrinsic and associational circuitry in monkey prefrontal cortex. J Comp Neurol. 376:614–630.
Ramsden BM, Hung CP, Roe AW. 2001. Real and illusory contour processing in area V1 of the primate: a cortical balancing act. Cereb Cortex. 11:648–665.
Rao SC, Toth LJ, Sur M. 1997. Optically imaged maps of orientation preference in primary visual cortex of cats and ferrets. J Comp Neurol. 387:358–370.
Read HL, Winer JA, Schreiner CE. 2001. Modular organization of intrinsic connections associated with spectral tuning in cat auditory cortex. Proc Natl Acad Sci U S A. 98:8042–8047.
Robins E, Smith DE, Eydt KM. 1956. The quantitative histochemistry of the cerebral cortex—I. J Neurochem. 1:54–67.
Rockland KS. 1985a. A reticular pattern of intrinsic connections in primate area V2 (area 18). J Comp Neurol. 235:467–478.
Rockland KS. 1985b. Anatomical organization of primary visual cortex (area 17) in the ferret. J Comp Neurol. 241:225–236.
Rockland KS, Lund JS. 1981. Anatomical banding of intrinsic connections of tree shrew striate cortex. IOVS. 20(Suppl):176 [abstract].
Rockland KS, Lund JS. 1982. Widespread periodic intrinsic connections in the tree shrew visual cortex. Science. 215:1532–1534.
Rockland KS, Lund JS. 1983. Intrinsic laminar lattice connections in primate visual cortex. J Comp Neurol. 216:303–318.
Rockland KS, Lund JS, Humphrey AL. 1982. Anatomical banding of intrinsic connections in striate cortex of tree shrews (Tupaia glis). J Comp Neurol. 209:41–58.
Ruthazer ES, Stryker MP. 1996. The role of activity in the development of long-range horizontal connections in area 17 of the ferret. J Neurosci. 16:7253–7269.
Sawaguchi T. 1994. Modular activation and suppression of neocortical activity in the monkey revealed by optical imaging. Neuroreport. 6:185–189.
Sawaguchi T. 1996. Functional modular organization of the primate prefrontal cortex for representing working memory process. Brain Res Cogn Brain Res. 5:157–163.
Schmidt KE, Goebel R, Löwel S, Singer W. 1997. The perceptual grouping criterion of colinearity is reflected by anisotropies of connections in the primary visual cortex. Eur J Neurosci. 9:1083–1089.
Sesma MA, Casagrande VA, Kaas JH. 1984. Cortical connections of area 17 in tree shrews. J Comp Neurol. 230:337–351.
Shapiro MB, Schein SJ, Monasterio FM. 1985. Regularity and structure of the spatial pattern of blue cones of macaque retina. J Am Stat Assoc. 80:803–812.
Sheth BR, Sharma J, Rao SC, Sur M. 1996. Orientation maps of subjective contours in visual cortex. Science. 274:2110–2115.
Shmuel A, Korman M, Sterkin A, Harel M, Ullman S, Malach R, Grinvald A. 2005. Retinotopic axis specificity and selective clustering of feedback projections from V2 to V1 in the owl monkey. J Neurosci. 25:2117–2131.
Shtoyerman E, Arieli A, Slovin H, Vanzetta I, Grinvald A. 2000. Long-term optical imaging and spectroscopy reveal mechanisms underlying

the intrinsic signal and stability of cortical maps in V1 of behaving monkeys. J Neurosci. 20:8111–8121.
Sincich LC, Blasdel GG. 2001. Oriented axon projections in primary visual cortex of the monkey. J Neurosci. 21:4416–4426.
Slovin H, Arieli A, Hildesheim R, Grinvald A. 2002. Long-term voltage-sensitive dye imaging reveals cortical dynamics in behaving monkeys. J Neurophysiol. 88:3421–3438.
Smirnov N. 1939. Sur les Écarts de la courbe de distribution empirique. Rec Math (Mat Sb). 6:3–26.
Springer MS, Murphy WJ, Eizirik E, O'Brien SJ. 2003. Placental mammal diversification and the Cretaceous-Tertiary boundary. Proc Natl Acad Sci U S A. 100:1056–1061.
Stettler DD, Das A, Bennett J, Gilbert CD. 2002. Lateral connectivity and contextual interactions in macaque primary visual cortex. Neuron. 36:739–760.
Tanaka K. 2003. Columns for complex visual object features in the inferotemporal cortex: clustering of cells with similar but slightly different stimulus selectivities. Cereb Cortex. 13:90–99.
Tani T, Yokoi I, Ito M, Tanaka S, Komatsu H. 2003. Functional organization of the cat visual cortex in relation to the representation of a uniform surface. J Neurophysiol. 89:1112–1125.
Tanigawa H, Wang Q, Fujita I. 2005. Organization of horizontal axons in the inferior temporal cortex and primary visual cortex of the macaque monkey. Cereb Cortex. 15:1887–1899.
Ts'o DY, Gilbert CD, Wiesel TN. 1986. Relationships between horizontal interactions and functional architecture in cat striate cortex as revealed by cross-correlation analysis. J Neurosci. 6: 1160–1170.
Tsunoda K, Yamane Y, Nishizaki M, Tanifuji M. 2001. Complex objects are represented in macaque inferotemporal cortex by the combination of feature columns. Nat Neurosci. 4:832–838.
Tusa RJ, Palmer LA, Rosenquist AC. 1978. The retinotopic organization of area 17 (striate cortex) in the cat. J Comp Neurol. 177: 213–236.
Tyler CJ, Dunlop SA, Lund RD, Harman AM, Dann JF, Beazley LD, Lund JS. 1998. Anatomical comparison of the macaque and marsupial visual cortex: common features that may reflect retention of essential cortical elements. J Comp Neurol. 400:449–468.
Van Essen DC, Newsome WT, Maunsell HR. 1984. The visual field representation in striate cortex of the macaque monkey: asymmetries, anisotropies, and individual variability. Vision Res. 24:429–448.
Van Hooser SD, Helmel JA, Chung S, Nelson SB. 2006. Lack of patchy horizontal connectivity in primary visual cortex of a mammal without orientation maps. J Neurosci. 26:7680–7692.
Versnel H, Mossop JE, Mrsic-Flogel TD, Ahmed B, Moore DR. 2002. Optical imaging of intrinsic signals in ferret auditory cortex: responses to narrowband sound stimuli. J Neurophysiol. 88:1545–1558.
Wallace MN, Bajwa S. 1991. Patchy intrinsic connections of the ferret primary auditory cortex. Neuroreport. 2:417–420.
Wallace MN, Kitzes LM, Jones EG. 1991. Intrinsic inter- and intralaminar connections and their relationship to the tonotopic map in cat primary auditory cortex. Exp Brain Res. 86:527–544.
Wang G, Tanaka K, Tanifuji M. 1996. Optical imaging of functional organization in the monkey inferotemporal cortex. Science. 272:1665–1668.
Wang Y, Xiao Y, Felleman DJ. 2007. V2 thin stripes contain spatially organized representations of achromatic luminance change. Cereb Cortex. 17:116–129.
Weller RE, White DM, Walton MMG. 2000. Intrinsic connections in the caudal subdivision of the dorsolateral area (DLC) in squirrel monkeys. J Comp Neurol. 420:52–69.
Xu X, Collins CE, Kaskan PM, Khaytin I, Kaas JH, Casagrande VA. 2004. Optical imaging of visually evoked responses in prosimian primates reveals conserved features of the middle temporal visual area. Proc Natl Acad Sci U S A. 101:2566–2571.
Xu X, Collins CE, Khaytin I, Kaas JH, Casagrande VA. 2006. Unequal representation of cardinal vs. oblique orientations in the middle temporal visual area. Proc Natl Acad Sci U S A. 103:17490–17495.
Yoshioka T, Blasdel GG, Levitt JB, Lund JS. 1996. Relation between patterns of intrinsic lateral connectivity, ocular dominance, and cytochrome oxidase-reactive regions in macaque monkey striate cortex. Cereb Cortex. 6:297–310.
Yoshioka T, Levitt JB, Lund JS. 1992. Intrinsic lattice connections of macaque monkey visual cortical area V4. J Neurosci. 12:2785–2802.